JACS
JOURNAL OF THE AMERICAN CHEMICAL SOCIETY
pubs.acs.org/JACS

Article

Mechanistic Studies of Oxidative Degradation in Diamine-Appended Metal−Organic Frameworks Exhibiting Cooperative CO_2 Capture

Shuoyan Xiong,[†] Alistair J. Sterling,[†] Nikolay V. Tkachenko,[†] Rhea-Donna Reyes, Hsinhan Tsai, Jaeheon Lee, Yu Chen, Yang Wang, Matthew N. Dods, David Lu, Ziting Zhu, Jonas Börgel, Jeong Won Kim, Abigail J. Schmeiser, Junyang Meng, Hiroyasu Furukawa, Aaron W. Peters, Bryan D. McCloskey, Jeffrey A. Reimer, Simon C. Weston, Martin Head-Gordon,* and Jeffrey R. Long*

Cite This: J. Am. Chem. Soc. 2025, 147, 25761−25778

Read Online

ACCESS | Metrics & More | Article Recommendations | Supporting Information

ABSTRACT: Understanding the impact of O_2 during a carbon capture process is vital for designing robust, cost-effective materials for carrying it out. However, mechanistic studies of the O_2-induced degradation of materials are not easily undertaken owing to the complex sequential reaction pathways that arise. Here, we report comprehensive mechanistic investigations of the O_2-induced degradation of diamine-appended metal−organic frameworks (MOFs) exhibiting cooperative CO_2 adsorption. Oxygen exposure experiments were performed on seven different diamine-appended MOFs, including e-2−Mg_2(dobpdc) (e-2 = *N*-ethylethylenediamine, dobpdc^{4-} = 4,4′-dioxidobiphenyl-3,3′-dicarboxylate), under various temperatures and O_2 pressures. These experiments show that diamine degradation inhibits CO_2 chemisorption and that the degradation rate is significantly influenced by the diamine structure. In contrast, the parent frameworks remain essentially intact upon O_2 exposure. Detailed characterization of O_2-exposed e-2−Mg_2(dobpdc) revealed the formation of various degradation products, including acetaldehyde, carbon dioxide, water, ethylamine, and other aldehyde- and imine-containing species. Together, these observations suggest that diamine degradation occurs via C−N bond cleavage through pathways involving C-centered radicals. Furthermore, computational evaluation of the initiation and propagation pathways for amine degradation in diamine-appended MOFs indicates that (i) degradation is likely initiated by OH•, (ii) carbon-centered radicals generated via radical transfer reactions react with O_2, leading to amine degradation, and (iii) the rate-limiting step of the degradation reactions likely involves O−O bond cleavage. Overall, these mechanistic insights could inform strategies for mitigating O_2-induced amine degradation in next-generation carbon capture technologies.

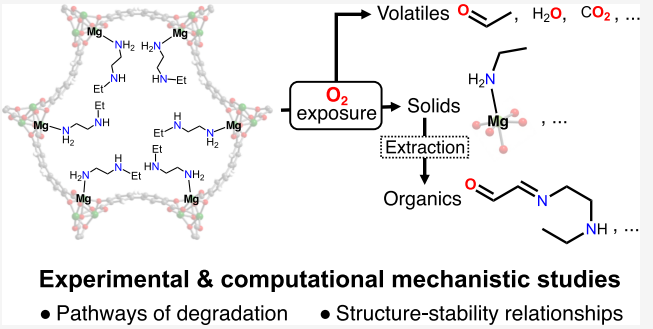

INTRODUCTION

Rapid economic and population growth since the 1970s has resulted in a doubling of global CO_2 emissions from fossil fuel combustion, associated with an increase in the atmospheric CO_2 concentration from ∼320 ppm to ∼420 ppm (the monthly average CO_2 concentration in Mauna Loa for December of 2024 was 425.4 ppm).[1−4] In efforts to reduce CO_2 emissions and ultimately meet the target set forth by the Paris Agreement of less than 2 °C of warming above preindustrial levels by the end of this century, the large-scale deployment of carbon capture technologies is expected to play a crucial role.[5−9] Currently, aqueous amine solutions are the most advanced and established systems for capturing CO_2. Despite their proven performance at the commercial scale, amine solutions suffer from volatilization, oxidation, energy-intensive regeneration, and low process efficiencies.[10] To overcome such limitations, alternative capture technologies, such as metal oxides and amine-based solid adsorbents, have been advanced in recent years.[3,11−14]

Over the past decade, we[15−23] and others[24−28] have demonstrated the potential of amine-appended metal−organic frameworks (MOFs) as transformative carbon capture materials (Figure 1a). In these materials, diamines or tetraamines are coordinated to the metal sites lining the channels within a honeycomb-type MOF. Insertion of one CO_2 molecule into a metal−N(amine) bond promotes additional CO_2 insertion into adjacent metal−N bonds, leading

Received: May 5, 2025
Revised: June 4, 2025
Accepted: June 5, 2025
Published: July 10, 2025

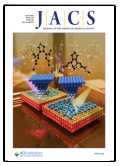

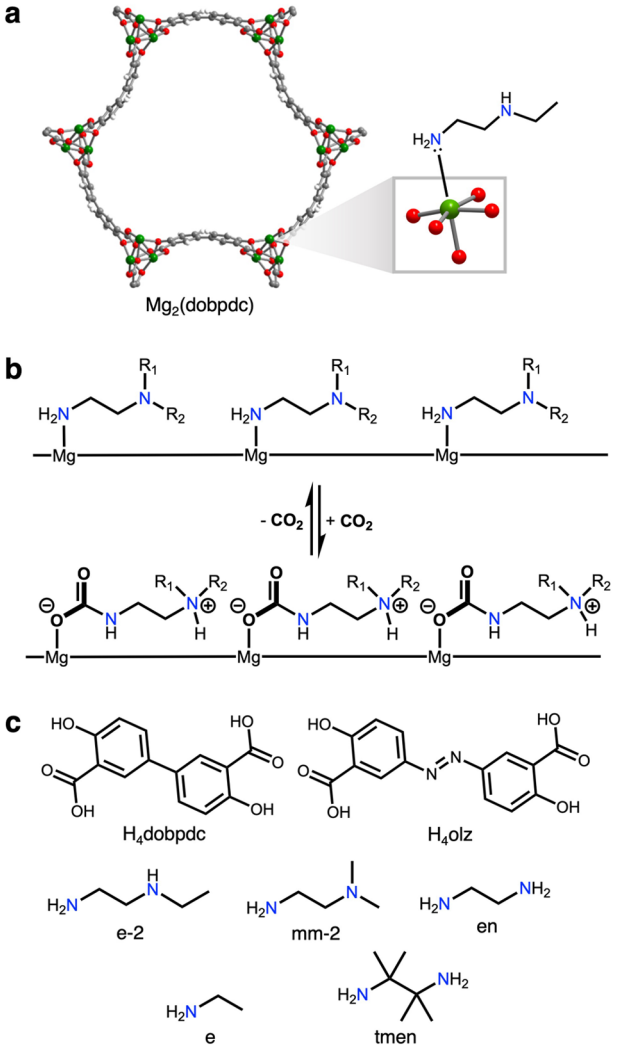

Figure 1. (a) Portion of the crystal structure of a representative Mg-based framework, Mg_2(dobpdc). Diamines can be appended to the coordinatively unsaturated Mg^{2+} cations. Green, gray, red and white represent Mg, C, O, and H atoms, respectively. (b) Schematic representation of cooperative CO_2 insertion into a diamine-appended framework to form ammonium carbamate chains. (c) Structures of the two linkers and five amines used in this study. Frameworks based on these two linkers, Mg_2(dobpdc) and Mg_2(olz), exhibit hexagonal pores with different diameters.

to the formation of one-dimensional ammonium carbamate chains (Figure 1b).[23,29,30] This cooperative CO_2 chemisorption results in exceptional CO_2 selectivity over other gases (e.g., N_2, O_2, CH_4) and sharp step-shaped adsorption profiles, where CO_2 uptake suddenly rises to near full capacity (i.e., one CO_2 per diamine) within a narrow temperature or pressure range, both in the presence and absence of water.[16,19,20] The ability to swing the full CO_2 adsorption capacity on and off the material with just a small change in temperature or pressure enables a high separation working capacity. Further, the CO_2-capture properties of these materials can be tuned by varying the appended amines, leading to adsorbents suitable for CO_2 capture from a variety of CO_2-containing gas streams, including crude natural gas (~0.7 bar CO_2),[17] emissions from coal-fired power plants (~15% CO_2),[18−20] and natural gas-fired combined cycle (NGCC) power plants (~4% CO_2),[16,21] and air (420 ppm of CO_2).[27,28]

Oxygen is a major component in a variety of CO_2-containing gas streams,[3,31−33] and therefore its impacts on the stability and lifetime of carbon capture materials must be carefully considered.[31,34−37] Oxidative degradation of aqueous amine systems has been extensively investigated.[38−47] More recently, there has been growing interest in understanding the impact of O_2 on solid carbon capture materials such as silica- or alumina-supported amine adsorbents.[31,37,48−59] These studies revealed O_2-induced amine degradation, which led to detrimental effects on the performance of the adsorbents. However, due to the structural complexity of these materials, precise and conclusive identification of the decomposition products, especially nonvolatile and amino species, remains challenging.

Despite their well-defined structures, the oxidative stability of amine-appended MOFs has not yet been investigated in detail, in contrast to the comprehensive studies that have been carried out on their adsorption mechanisms, adsorption kinetics, and stability under humid conditions.[16,18,19,21,30] Given that the unique cooperative mechanism relies upon continuous, ordered chains of amines running along the one-dimensional pores, O_2-induced amine degradation, if occurring, could dramatically affect the CO_2 capture performance of these materials. A preliminary study of a tetraamine-appended framework, 3-4-3−Mg_2(dobpdc) (3-4-3 = *N*,*N*′-bis(3-aminopropyl)-1,4-diaminobutane; $dobpdc^{4-}$ = 4,4′-dioxidobiphenyl-3,3′-dicarboxylate), revealed moderate capacity loss after air exposure at 100 °C for 12 h.[21] For a commercial application, degradation at this level would be unacceptable if O_2 exposure at such an elevated temperature were to occur in every adsorption−desorption cycle over a period of many months or years.[8,35,60,61] Therefore, it is crucial to examine whether the amines or frameworks degrade upon exposure to O_2 and how the amine and framework structures affect oxidative stability, as well as the O_2-induced degradation pathways of these materials. The results of such studies could pave the way for effectively mitigating degradation, significantly lowering the cost of a separation process.

Herein, we report detailed mechanistic investigations focused on the O_2-induced degradation of diamine-appended metal−organic frameworks, including an evaluation of the impact of O_2 exposure on adsorbent performance, the recognition of diamine degradation, and, for the first time, the identification of the molecular structures of several key degradation products. Combining further experimental findings and computational calculations, we also propose degradation pathways for how the O_2-induced degradation is initiated and propagated in the pores of the frameworks.

RESULTS AND DISCUSSION

Diamine-appended frameworks were prepared and characterized according to published procedures (see the Supporting Information, Section S2 for details).[15,17,18,22] Briefly, Mg_2(dobpdc) and Mg_2(olz) (olz^{4-} = (*E*)-5,5′-(diazene-1,2-diyl)bis(2-oxidobenzoate) were synthesized via solvothermal methods from $Mg(NO_3)_2{\cdot}6H_2O$ and the corresponding linker precursor, H_4dobpdc or H_4olz, respectively (Figure 1c). Next, the methanol-solvated MOF was soaked in a diamine-containing toluene solution for 18 h, and the resulting solid was collected by filtration and activated (i.e., desolvated) by heating under flowing argon. The crystallinity and porosity of the bare and diamine-appended frameworks were confirmed by powder X-ray diffraction analysis and N_2 adsorption isotherm measurements at 77 K. The amount of diamine loaded into the

https://doi.org/10.1021/jacs.5c07551
J. Am. Chem. Soc. 2025, 147, 25761−25778

activated sample was determined based on ^{1}H nuclear magnetic resonance (NMR) measurements of acid-digested samples (i.e., treatment with 35 wt % deuterium chloride solution in deuterated water, denoted as "DCl digestion"). Prior to evaluating the oxidative stability of the diamine-appended frameworks, thermogravimetric measurements of the materials were performed under a constant pressure of dry CO_2 flow (CO_2 isobar) to estimate the CO_2 adsorption capacity through the weight change of the material, along with the step temperature at which this uptake occurs.

Air Stability of e-2–Mg_2(dobpdc). An ethyl ethylenediamine (e-2) appended framework, e-2–Mg_2(dobpdc), was selected as the reference adsorbent because e-2 is one of the simplest diamines and CO_2 adsorption behaviors of e-2–Mg_2(dobpdc) were well studied previously in our laboratory (Figure 1c).[3,17] To estimate the CO_2 adsorption capacity, a CO_2 isobar for freshly prepared and activated (denoted as "pristine") e-2–Mg_2(dobpdc) was collected under a pure CO_2 stream. The isobar did not show a significant weight change when the temperature was higher than 130 °C, while a large, step-shaped weight increase was observed at around 120 °C due to CO_2 adsorption in the material (Figure 2a). The amount of CO_2 adsorbed corresponds to one CO_2 per diamine, which is consistent with our previous results.[17]

The pristine e-2–Mg_2(dobpdc) sample was exposed to dry air at ambient temperature (~25 °C) for 60 days to evaluate the air stability of the amine-appended frameworks (see the Supporting Information, Section S2.2 for detailed procedures). While moderate degradation was observed after 60 days of air exposure, as evidenced by the ~15% decrease in the amount of CO_2 adsorbed in the CO_2 isobar of the air-exposed sample compared to that of the pristine material (Figure 2a), the lengthy nature of this experiment prevents evaluation of multiple samples in a time-efficient manner. These observations prompted us to conduct O_2 exposure experiments under harsher conditions (i.e., higher temperature and O_2 concentration, see the Supporting Information, Section S3 for details).

Accelerated O_2 Exposure Experiments with e-2–Mg_2(dobpdc). Upon exposing e-2–Mg_2(dobpdc) to atmospheric pressure of dry O_2 at 100 °C for 5 days (see the Supporting Information, Section S2.3 for detailed procedures), a significant decrease in the CO_2 adsorption capacity and broadening of the adsorption step were observed in the corresponding CO_2 isobar (Figure 2b), indicating faster and more severe degradation than that observed after 60 days of exposure to ambient air, as described above. This is in sharp contrast to the sample pretreated by heating at 100 °C for 10 days under argon, for which the CO_2 isobar profile exhibited only minor differences from that of the pristine sample. Therefore, the presence of O_2 is the primary factor in the loss of CO_2 adsorption capacity. This loss is likely due to changes in the structure of e-2 and/or crystallinity and porosity of the framework. To further evaluate and deconvolute the impact of O_2 exposure on the appended diamine and the host framework, a set of techniques was employed to characterize e-2–Mg_2(dobpdc) before and after O_2 exposure.

Analysis of acid-digested samples for the pristine and O_2-exposed e-2–Mg_2(dobpdc) via solution NMR spectroscopy revealed decreases in the ratio of diamine to organic linker upon O_2 exposure and the appearance of several new resonances close to the resonances for e-2 in the aliphatic region of corresponding ^{1}H NMR spectra (Figure 2c). Compared with the sample exposed to O_2 for 5 days, the

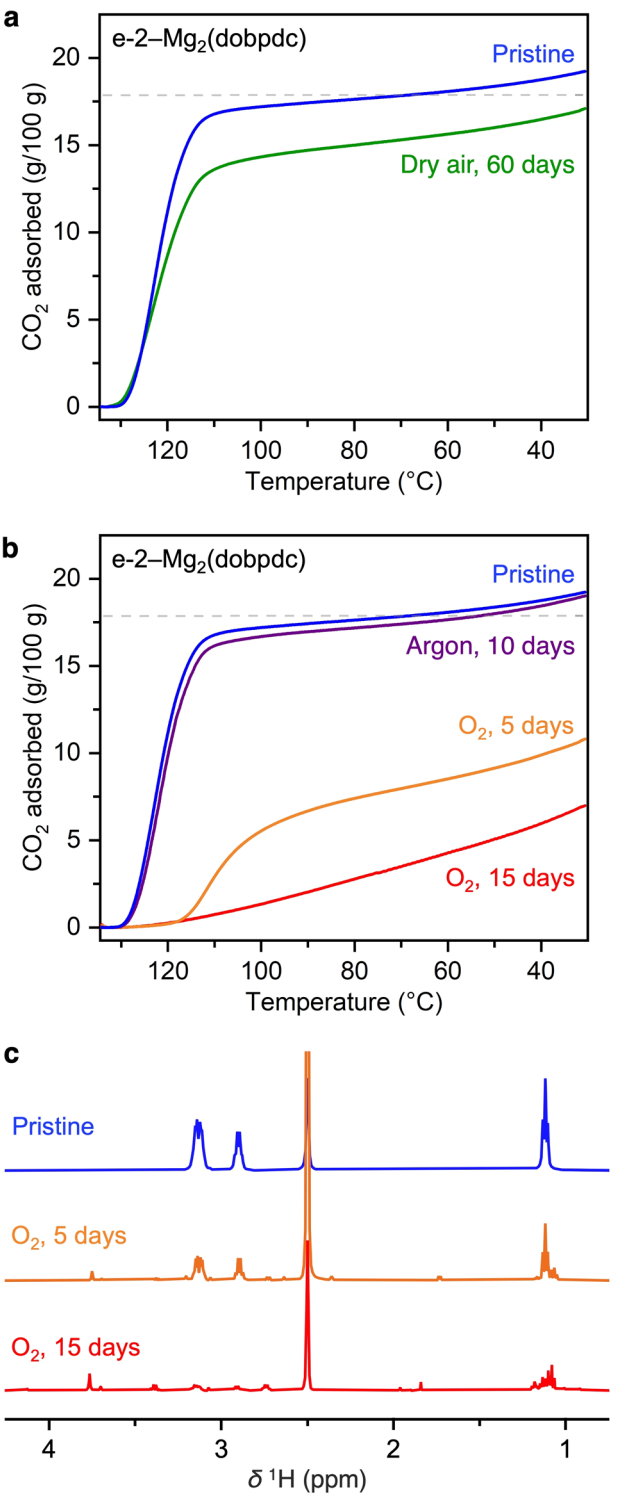

Figure 2. (a) Pure CO_2 isobars of e-2–Mg_2(dobpdc) after exposure to dry air at ~25 °C for 60 days. (b) Pure CO_2 isobars of e-2–Mg_2(dobpdc) after exposure to O_2 for 5 and 15 days at 100 °C or to argon for 10 days at 100 °C. In panels (a, b), a CO_2 isobar for the pristine e-2–Mg_2(dobpdc) sample is overlaid as a reference, and the gray dashed line corresponds to the full CO_2 adsorption capacity (1 CO_2 per diamine). (c) Aliphatic region of the solution ^{1}H NMR spectra of DCl-digested species from pristine e-2–Mg_2(dobpdc) and e-2–Mg_2(dobpdc) after 5 and 15 days of O_2 exposure at 100 °C (solvent: DMSO-d_6). The peak intensity in the spectra is normalized based on the organic linker peak that appeared in the aromatic region (not shown).

https://doi.org/10.1021/jacs.5c07551
J. Am. Chem. Soc. 2025, 147, 25761–25778

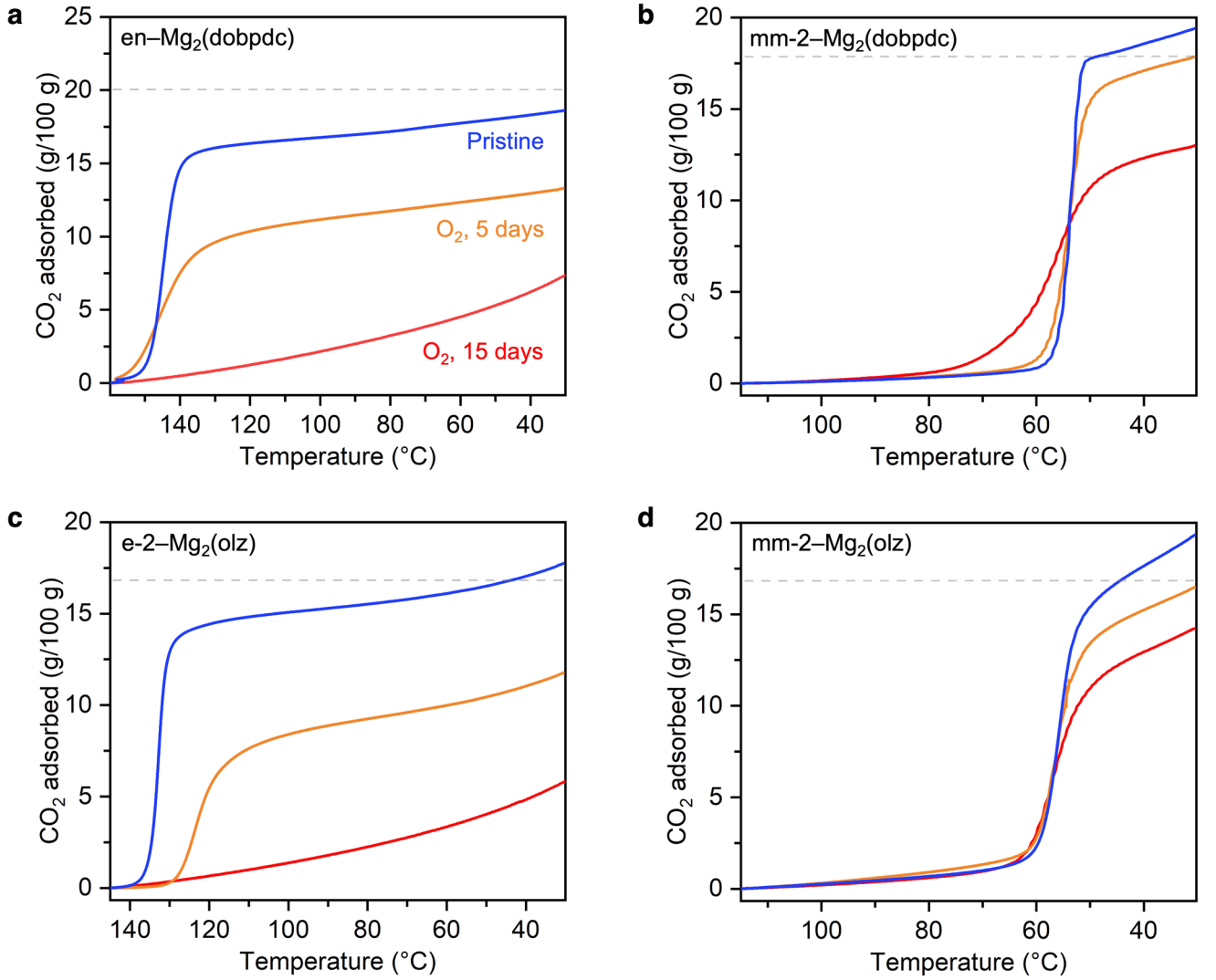

Figure 3. (a–d) Pure CO_2 isobars of four diamine-appended frameworks after O_2 exposure at 100 °C for the indicated time intervals (orange: after 5 days of O_2 exposure, red: after 15 days of O_2 exposure, as shown in panel (a). For references, the CO_2 isobars for the corresponding pristine samples are overlaid (blue). Gray dashed lines correspond to the full CO_2 adsorption capacity (1 CO_2 per diamine).

intensity of resonances for e-2 was further decreased when the sample was exposed to O_2 for 15 days, along with an increase in the intensity of new resonances. In contrast, a significant difference in the aromatic region of the ^{1}H NMR spectra, associated with the dobpdc^{4-} linker, was not observed upon O_2 exposure (Figure S9). These findings indicate that O_2 exposure of e-2–Mg_2(dobpdc) predominantly degrades the appended diamine molecules.

The structural integrity of the framework after 15 days of O_2 exposure was further examined using powder X-ray diffraction (λ = 1.5418 Å) and surface area analysis. The X-ray diffraction pattern of the oxidized sample was nearly identical to that of the pristine sample (Figure S25), as expected from NMR analysis of acid-digested samples that displayed an almost identical spectral profile in the aromatic region. The O_2-exposed sample also exhibits a surface area similar to that of the pristine material (Figure S29). Because the precise composition of chemical species in the pores is not available, we are not able to determine whether the porosity change of the Mg_2(dobpdc) framework itself is negligible after the O_2 exposure. However, it is reasonable to conclude that the O_2 stability of the framework is significantly higher than the appended diamines.

Benchmarking Oxidative Stability. The foregoing studies indicate that O_2 exposure causes partial degradation of the diamine in e-2–Mg_2(dobpdc) while the framework structure remains intact over the course of the experiments. It should also be noted that similar new resonances were found in the ^{1}H NMR spectrum of the acid-digested sample of e-2–Mg_2(dobpdc) after 60 days of ambient air exposure (Figure S10). The formation of similar products during exposure to ambient air and accelerated exposure conditions suggests that the degradation of e-2 should follow similar degradation pathways regardless of the temperature and the oxygen concentration. Therefore, these accelerated conditions (pure O_2 and 100 °C) should be suitable for evaluating the oxidative stability of the diamine-appended frameworks. Employing these conditions, we next performed O_2 exposure experiments with four additional diamine-appended frameworks, ethylenediamine (en)- and *N,N*-dimethyl-ethylenediamine (mm-2)-appended Mg_2(dobpdc), and e-2- and mm-2-appended Mg_2(olz). In these materials, each Mg center is coordinated by a primary amino group, and the spacing between two amino

https://doi.org/10.1021/jacs.5c07551
J. Am. Chem. Soc. 2025, 147, 25761–25778

groups remains the same (Figure 1b,c). Meanwhile, we systematically varied the functionality of the dangling amino group from primary (en), through secondary (e-2) to tertiary (mm-2).

First, we collected CO_2 isobars for these materials to evaluate how the structures of diamines and frameworks affect the CO_2 adsorption capacity after O_2 exposure. As expected, all pristine materials displayed a single-step isobar upon CO_2 adsorption with nearly full capacity (Figures 1b and 3).[16−18,22,29] After 5 days of O_2 exposure at 100 °C, isobars for the en- and e-2-appended frameworks exhibited a shallow step, and their CO_2 adsorption capacity dropped to roughly half of the original values. In contrast, the differences observed in CO_2 isobars for the mm-2-appended frameworks were much smaller (Figure 3), and these isobars exhibited a distinctive step originating from CO_2 adsorption even after a 15-day O_2 exposure. These findings clearly demonstrate that O_2 exposure induces the loss of CO_2 adsorption capacity, while adsorbents featuring certain diamine structures are likely less susceptible to O_2-induced degradation (we will discuss this point later in detail).

Similar to e-2−Mg_2(dobpdc), diamine degradation for these four adsorbents, en−Mg_2(dobpdc), mm-2−Mg_2(dobpdc), e-2−Mg_2(olz), and mm-2−Mg_2(olz), was confirmed by ^{1}H NMR analysis of corresponding acid-digested samples of O_2-exposed materials (Figures S34−S38 and Table S2). The most stable diamine-appended frameworks were the mm-2-appended versions as they exhibited the least diamine loss among these adsorbents. This is consistent with the isobar analyses, where they featured a smaller loss of CO_2 adsorption capacity upon O_2 exposure compared to other frameworks.

In contrast to the varying levels of performance loss with diamine degradation, the host frameworks all remained intact after accelerated O_2-exposure experiments regardless of the diamines appended, as evidenced by the minute changes in the aromatic region of the NMR spectra of the acid-digested samples, which contain resonances for the linker. This is also supported by the retention of high porosity, as estimated by N_2 isotherm measurements at 77 K, and the presence of sharp powder X-ray diffraction peaks after O_2 exposure (Figures S25−S31). These findings are consistent with the above studies on e-2−Mg_2(dobpdc). The oxidative stability of the framework materials is also supported by morphology observations of crystalline powder samples using high-angle annular dark-field scanning transmission electron microscopy (HAADF-STEM) (Figures S32 and S33). The similarity in the images obtained for pristine and O_2-exposed samples indicates that the frameworks are not significantly influenced by O_2 exposure at 100 °C for 15 days.

Impact of O_2-Induced Amine Degradation on the CO_2 Adsorption Mechanism. It is likely that if the appended diamine molecules were degraded, CO_2 chemisorption relying on cooperative CO_2 insertion into the Mg−N(diamine) bond would be inhibited, although the degraded materials should still physisorb CO_2 molecules to some extent. We have previously reported that ^{13}C solid-state NMR spectra acquired by direct excitation display resonances for chemisorbed and physisorbed $^{13}CO_2$, at ∼160 and 125 ppm, respectively.[30] To assess whether the CO_2 chemisorption ability of the O_2-exposed materials is retained, we collected direct ^{13}C magic angle spinning (MAS) solid-state NMR (^{1}H decoupled) spectra of the $^{13}CO_2$-dosed diamine-appended materials before and after 15 days of O_2 exposure at 100 °C.[29,30]

The ^{13}C MAS solid-state NMR spectrum of $^{13}CO_2$-dosed pristine e-2−Mg_2(dobpdc) exhibited resonances at ∼162 and ∼125 ppm, which are assigned to chemisorbed and physisorbed $^{13}CO_2$, respectively, based on our previous reports (Figure 4a, blue line).[30] After O_2 exposure at 100 °C for 15 days, the resulting e-2−Mg_2(dobpdc) sample exhibited only one major resonance peak (∼125 ppm) in the ^{13}C MAS solid-state NMR spectrum, indicating that most of the CO_2 is physisorbed in the pores. This scenario suggests that O_2 exposure inhibits CO_2 chemisorption. The disappearance of the resonance at ∼162 ppm associated with chemisorbed CO_2 was also observed with the samples of en−Mg_2(dobpdc) and e-2−Mg_2(olz) after 15 days of O_2 exposure at 100 °C (Figure 4b,c), consistent with the significant decrease of CO_2 adsorption capacity and the disappearance of the sharp adsorption steps in the corresponding CO_2 isobars (Figure 3). Notably, when $^{13}CO_2$ is dosed into the O_2-exposed mm-2−Mg_2(olz) sample, which still features step-shaped CO_2 adsorption in its isobar, the resonances originating from the chemisorbed $^{13}CO_2$ species were observed (Figures 3d and 4d). These results again highlight the high O_2 tolerance of mm-2-appended frameworks.

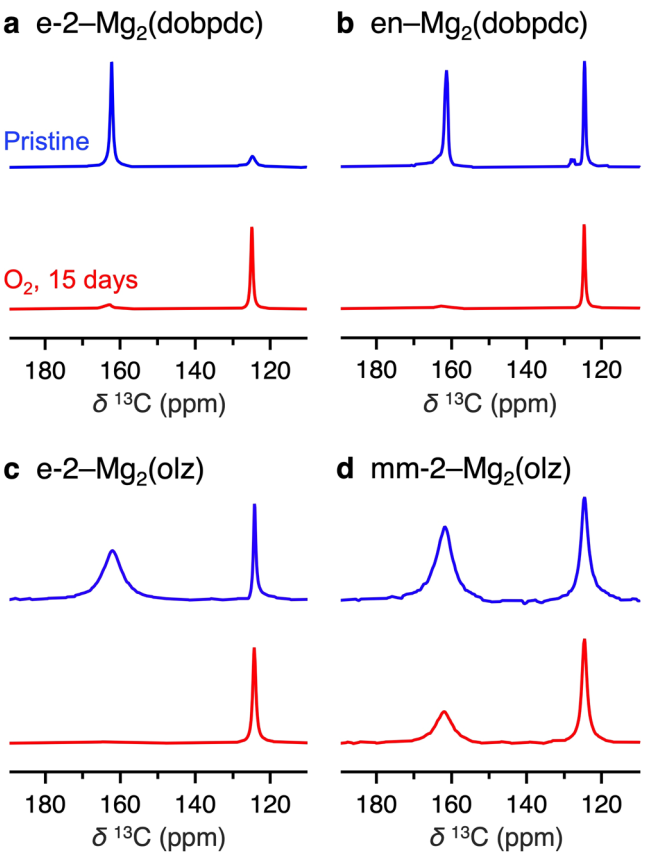

Figure 4. (a−d) Direct solid-state ^{13}C MAS NMR (^{1}H decoupled) spectra of $^{13}CO_2$-dosed diamine-appended frameworks without O_2 exposure (blue) and after 15 days of O_2 exposure at 100 °C (red). See the Supporting Information, Section S2.5 for detailed NMR parameters. The peaks at ∼160 and ∼125 ppm are assigned to chemisorbed and physisorbed $^{13}CO_2$, respectively. Carbon-13 CO_2 gas was dosed at ∼1 bar. Solid-state NMR experiments, including $^{13}CO_2$ dosing, were performed at room temperature.

Product Identification for O_2-Induced Diamine Degradation in e-2−Mg_2(dobpdc). The aforementioned studies

https://doi.org/10.1021/jacs.5c07551
J. Am. Chem. Soc. 2025, 147, 25761−25778

reveal that the primary reason for the loss of CO_2 adsorption capacity in diamine-appended frameworks after O_2 exposure is diamine degradation; however, the identity of the products from diamine degradation in the frameworks, as well as the corresponding degradation mechanism, remains elusive. We next conducted a series of experimental studies to identify the molecular structures of degradation products using e-2–Mg_2(dobpdc) as the adsorbent.

Degradation Products Remaining in the Framework. To identify the degradation products accurately, it is critical to select characterization techniques that do not require workup procedures that may trigger further reactions. For instance, while NMR analysis of acid-digested samples is a convenient way to confirm the formation of new species, the new species observed do not necessarily represent the actual products of O_2-induced degradation, because a strong acid like deuterium chloride is also highly reactive and may alter the degraded species. To overcome this problem and identify the exact degradation products remaining in the framework pores, we employed cross-polarization ^{13}C solid-state NMR spectroscopy, which allowed us to characterize O_2-exposed adsorbents in bulk.

The cross-polarization ^{13}C solid-state NMR spectrum of the oxidized e-2–Mg_2(dobpdc) sample was collected to compare with that of the pristine sample. Similar to the solution NMR experiments, multiple new resonance peaks were observed in the aliphatic region after O_2 exposure (Figure 5a). Notably, two of the new resonances located at ∼16 and ∼36 ppm are reminiscent of the chemical shifts of ethylamine in solution NMR spectra,[62] which could be generated by amine oxidation through C–N bond cleavage.[63,64] Therefore, an ethylamine-appended framework, e–Mg_2(dobpdc), was prepared as a model compound, although the ethylamine loading (i.e., the ratio of ethylamine to the Mg site) in the pores was roughly two-thirds due to the competing binding of tetrahydrofuran (THF) to the Mg sites (Figure S43, see the Supporting Information, Section S4 for details). As shown in Figure 5, the cross-polarization ^{13}C solid-state NMR spectrum for e–Mg_2(dobpdc) exhibited four resonances in the aliphatic region, two of which were assigned to the appended ethylamine in the Mg_2(dobpdc) framework, and the other two are resonances for the remaining THF used for ethylamine appending (marked with asterisks).[65] Considering that both e–Mg_2(dobpdc) and O_2-exposed e-2–Mg_2(dobpdc) samples displayed nearly identical resonances assignable to ethylamine, ethylamine is determined to be one of the degradation products generated during O_2-exposure of e-2–Mg_2(dobpdc).

In the aromatic region of the ^{13}C solid-state NMR spectra, no significant difference between pristine and O_2-exposed e-2–Mg_2(dobpdc) was observed in the resonances corresponding to carbons on the dobpdc^{4-} linker (Figure 5b). This result is consistent with the oxidative stability of the framework structures, as shown by acid digestion NMR and X-ray diffraction analyses. One noticeable difference in the aromatic region is that the O_2-exposed adsorbents display two new resonances at 160 and 145 ppm, within the range of resonances for the C=N functionality.[53,54] This is reminiscent of the formation of carbonyl and imino species resulting from O_2-induced degradation that has been proposed for poly(ethylenimine) (PEI) on an alumina support based on new infrared bands that appeared at 1600–1700 cm^{-1} (Figure S39).[37] However, the molecular structures of these C=N-containing species remain elusive due to the limitations of solid-state characterization techniques (i.e., solid-state NMR spectroscopy and infrared spectroscopy) in structure determination.

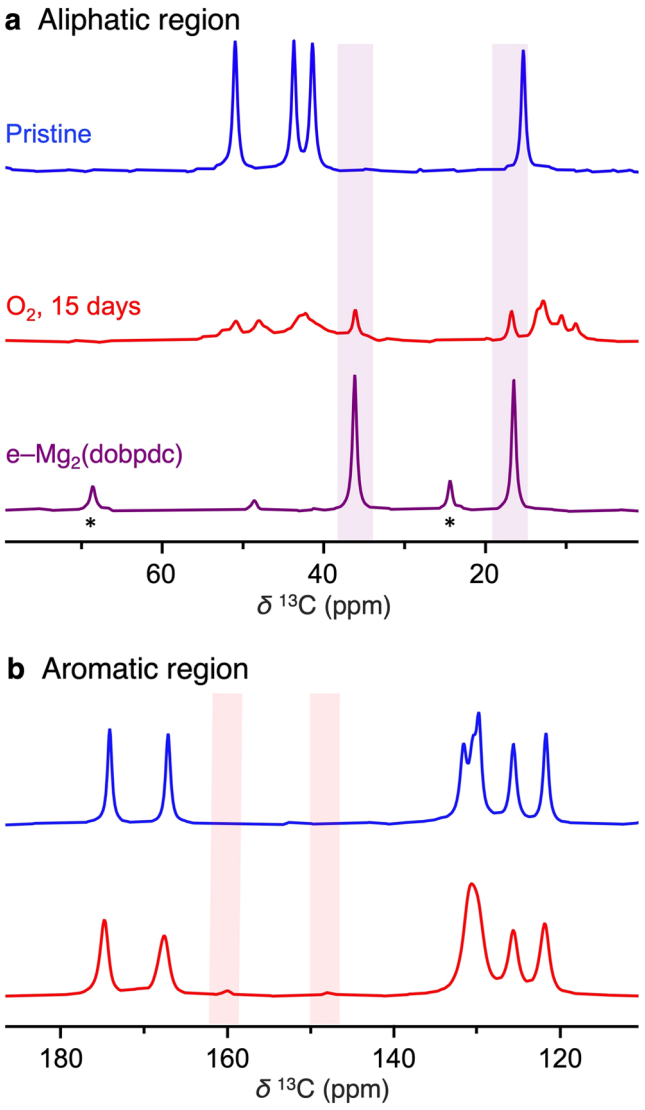

Figure 5. (a) Cross-polarization ^{13}C solid-state NMR spectra (aliphatic region) of the remaining solids from pristine e-2–Mg_2(dobpdc) (blue), O_2-exposed e-2–Mg_2(dobpdc) (red), and independently prepared e–Mg_2(dobpdc) (purple). Two resonances, highlighted in purple, are assigned to two carbons in ethylamine. (b) Cross-polarization ^{13}C solid-state NMR spectra (aromatic region) of the remaining solids from pristine e-2–Mg_2(dobpdc) (blue) and O_2-exposed e-2–Mg_2(dobpdc) (red). Two resonances, highlighted in red, are proposed to be associated with imino species. Asterisk marks indicate the presence of the remaining THF in the pores (see the text for details). See the Supporting Information, Section S2.5 for detailed NMR parameters.

Organic Species Extracted from the Framework. To further probe the identity of degradation products that cannot be recognized via solid-state NMR analysis, we extracted the organic species with methanol from O_2-exposed e-2–Mg_2(dobpdc). Unlike DCl digestion, methanol soaking can extract organic species from the pores without breaking down the framework structure into corresponding metal salts and linkers. Although extraction is less efficient than digestion for accurate quantification (Figure S40), the extracts are suitable

https://doi.org/10.1021/jacs.5c07551
J. Am. Chem. Soc. 2025, 147, 25761–25778

for qualitative analysis using gas chromatography with mass spectrometry detection (GC-MS).

For the major component observed in the GC plot of the extracts from $^{16}O_2$-exposed e-2−Mg_2(dobpdc), we found that its mass-to-charge (m/z) ratio was 128, which is assigned to its molecular weight. Notably, the extracts from the $^{18}O_2$-exposed sample exhibited a larger value of m/z = 130 (Figure 6a,b).

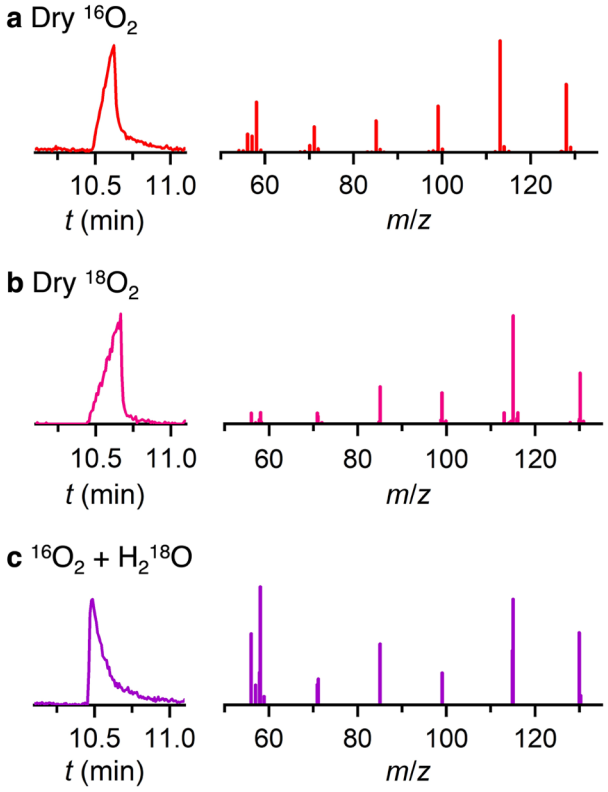

Figure 6. Gas chromatograms (left) and corresponding mass spectra (right) for m/z = 128 and 130 species observed in GC-MS analysis. The organic species were extracted with methanol from the remaining solids of e-2−Mg_2(dobpdc) after exposure to dry $^{16}O_2$ (a) and dry $^{18}O_2$ (b) at 100 °C for 15 days and $^{16}O_2$ containing $H_2{}^{18}O$ (c) at 100 °C for 7 days.

Considering their similar m/z patterns, it is presumed that these species are essentially the same, and the difference in the mass comes from the single oxygen atom, ^{16}O or ^{18}O, depending on the O_2 source. Based on the structure of e-2, as well as our hypothesis that formation of imine species and occurrence of O_2-induced C−N bond cleavage generate acetaldehyde and ethylamine, we propose the formation of aminoacetaldehyde or iminoacetaldehyde derivatives (Figure S51) that may be generated via combined processes involving C−N bond cleavage, aldehyde oxidation, decarboxylation, and/or imine condensation. We note that organic species with m/z = 169, containing ^{16}O (171 for the product containing ^{18}O), and 194 were also observed in GC-MS analyses (Figures S48 and S49), where these imino species could be formed by a similar mechanism as the organic species with m/z = 128.

It is also likely that water, inevitably present in practical carbon capture processes, is involved in the degradation mechanisms. Therefore, we examined the role of water in aldehyde formation by exposing a sample of e-2−Mg_2(dobpdc) to $^{16}O_2$ in the presence of $H_2{}^{18}O$ and then performing a methanol extraction (see the Supporting Information, Section S6 for detailed procedures). The appearance of the species with m/z = 130 as the major component in the GC-MS data suggests that at least one pathway for aldehyde formation involves water. One possible pathway is through the hydrolysis of imino species generated upon O_2 exposure in the presence of water (Figure S50).

Volatile Degradation Products in the Gas Phase. The foregoing studies identified several amine degradation products with low volatility. We therefore sought to determine whether O_2 exposure leads to the formation of gas-phase degradation products, and if so, to identify their molecular structures. To do this, mass spectrometry was used to analyze the volatile species from $^{16}O_2$ and $^{18}O_2$ exposure experiments with e-2−Mg_2(dobpdc) (see the Supporting Information, Section S7 for experimental details).

As a typical example, we describe the analysis of the gaseous species with a mass-to-charge ratio of m/z = 44 observed in the $^{16}O_2$ exposure experiment (Figure S54). In the region of m/z = 40−50, this particular m/z ratio is the sole observed signal in the $^{16}O_2$ exposure experiment (100 °C, 15 days, dry O_2 exposure) and could correspond to CO_2 or acetaldehyde. Notably, the volatiles from the analogous $^{18}O_2$ exposure experiment exhibited three signals with different m/z ratios (44, 46, and 48) in the same region. Given that the only source of an ^{18}O atom is $^{18}O_2$, the volatiles with m/z = 46 and 48 should result from reactions involving O_2. The ^{18}O-labeled compound with m/z = 46 is likely acetaldehyde, containing just one ^{18}O atom. Similarly, the volatile species with m/z = 48 should have two ^{18}O atoms. Thus, a plausible explanation is that $C^{18}O_2$ was generated by further oxidation of acetaldehyde or other aldehyde-containing species followed by decarboxylation. The m/z = 44 signal observed in the $^{18}O_2$ experiment is unlikely to be related to a labeled oxygen atom, but rather is most likely to be a result of CO_2 from air entering the system during the operation.

The formation of water is indicated by the observation of m/z = 19 and 20 signals in the experiments with $^{18}O_2$ and the observation of m/z = 17 and 18 signals when $^{16}O_2$ was used for the accelerated degradation with dry O_2 exposure at 100 °C for 15 days (Figure S55). During O_2 exposure, H_2O may be generated via hydrogen atom transfer (HAT) between a peroxide species and an amino species, or through a reaction between an aldehyde species and an amino species.

Experimental Investigations of the Mechanisms of e-2 Degradation in the Frameworks. It is known that amine oxidation processes typically occur via radical pathways, where the radical is often located on the nitrogen atom or an adjacent carbon atom (α-amino carbon).[66−69] Importantly, the formation of C-centered radicals can be inhibited by full substitution of the α-amino carbon atoms. If oxidative degradation of diamines in the frameworks involves C-centered radicals, functionalization of the α-amino carbon atoms should enhance oxidative stability. To test this hypothesis, we appended the Mg_2(dobpdc) framework with 2,3-diamino-2,3-dimethylbutane (tmen), for which the α-amino carbon atoms are fully substituted, in a similar manner to the other amine-appended frameworks (see the Supporting Information, Section S8 for detailed procedures).

Although we made various attempts to achieve the full diamine loading (i.e., 1 tmen per Mg site), we only reached ~80%, possibly due to the high rigidity of the diamine structure, which could make it difficult to be accommodated in the pores. After 10 days of O_2 exposure at 100 °C, the ^1H

https://doi.org/10.1021/jacs.5c07551
J. Am. Chem. Soc. 2025, 147, 25761−25778

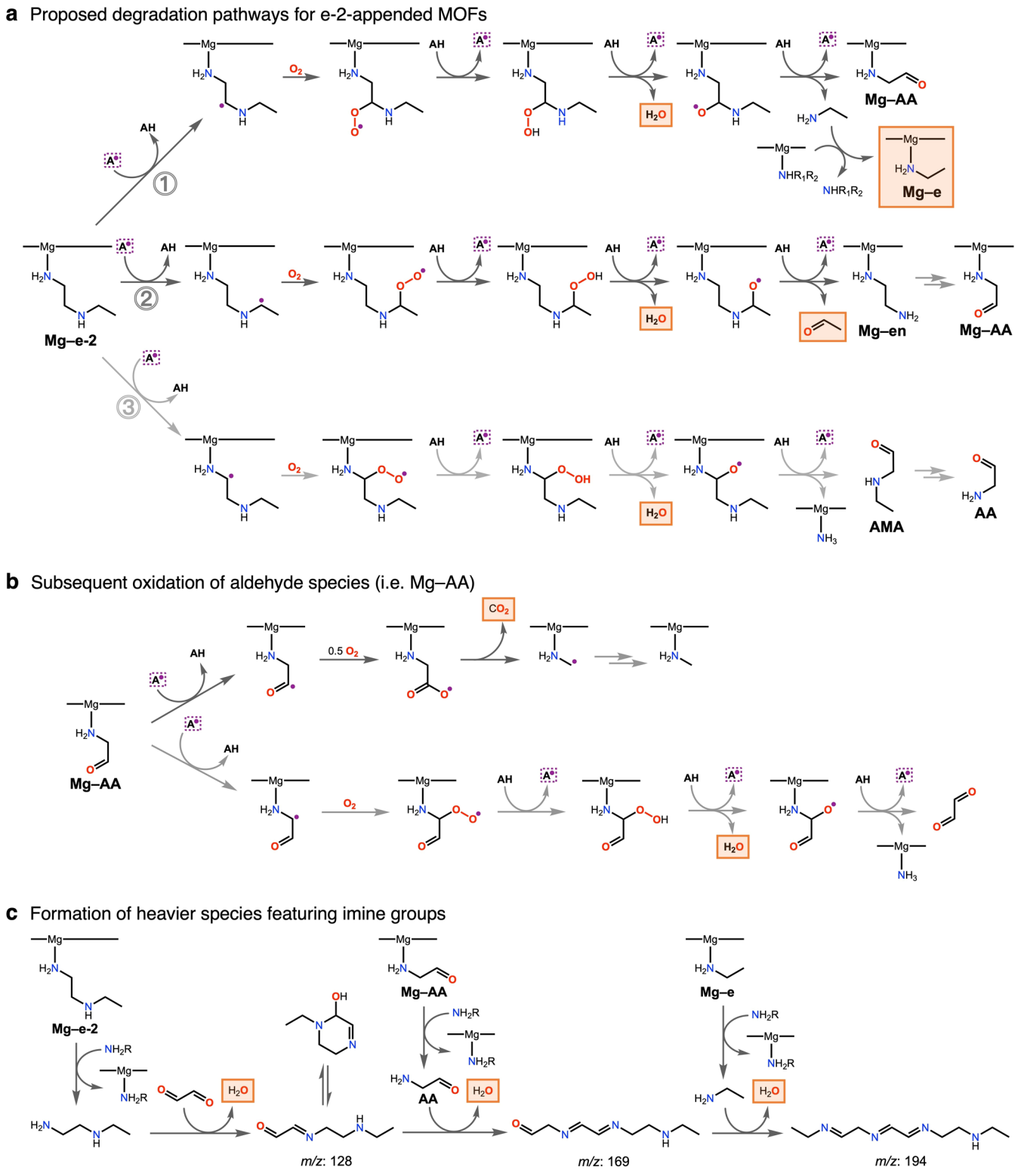

Figure 7. Possible oxidative degradation pathways via C−N bond cleavage of e-2 appended to the framework (a) and subsequent reactions (b, c). Reactions with light gray arrows are likely to occur but unconfirmed experimentally in this study. Species in an orange rectangle have been observed experimentally. While imino species with m/z = 128, 169, and 194 were also observed experimentally, their exact molecular structures are difficult to determine due to the existence of multiple isomers, as listed in Figure S51. Panel (c) represents one possible pathway for the formation of one set of these imino species. Oxygen atoms originating from O_2 and unpaired electrons are highlighted in red and purple, respectively. Radical species, shown as $A^{\bullet}$ and highlighted in dashed purple rectangles, could be initiators ($X^{\bullet}$, typically $OH^{\bullet}$) and radical species generated during oxidation.

NMR spectrum of the acid-digested sample for O_2-exposed tmen−Mg_2(dobpdc) was nearly identical to that of the corresponding pristine sample (Figures S58 and S59), in contrast to e-2-appended frameworks. Further, the diamine loading of this material was not influenced by the accelerated oxidation conditions, indicating a high oxidative stability for

https://doi.org/10.1021/jacs.5c07551
J. Am. Chem. Soc. 2025, 147, 25761−25778

tmen. To exclude the possibility that the high stability originates from the lower initial amine loading, the framework with a larger pore diameter, Mg_2(olz), was also appended with tmen using analogous procedures to e-2−Mg_2(olz), affording tmen−Mg_2(olz), which indeed achieved ∼99% tmen loading (Figure S60, see the Supporting Information, Section S8 for detailed procedures). Notably, tmen−Mg_2(olz) held ∼98% of tmen without degradation in the pores of the framework after 10 days of O_2 exposure at 100 °C (Figures S60 and S61). These findings clearly demonstrate that amine degradation can be efficiently suppressed by deliberately functionalizing diamine molecules to inhibit the formation of C-centered radicals. Therefore, O_2-induced diamine degradation in the pores of the frameworks likely involves C-centered radicals, although the intermediacy of N-centered radical species cannot be ruled out.

Given that C-centered radicals are likely involved in the oxidative degradation process, the next question is how such radicals are generated, specifically through either photochemical or chemical processes. If the major pathway for radical generation involved light-induced singlet O_2 or ozone, O_2-induced degradation of diamines should be slowed down by maintaining a dark environment during O_2 exposure. Therefore, we compared the profile of CO_2 isobars for e-2−Mg_2(dobpdc) after O_2 exposure in the dark and under light. Relative to the regular oxidation experiments, the sample after O_2 exposure in the dark for 5 days displayed only marginally higher CO_2 uptake, indicating that light does not play a critical role in diamine degradation (Figure S41).

It has also been proposed that a trace amount (i.e., ppm-level) of redox-active metals can cause amine degradation in liquid and solid sorbents.[70−73] This is because these metals may react with O_2 to generate peroxide radical anions or hydroxy radicals that could react with the amines to initiate oxidative degradation.[74,75] We therefore evaluated the amount of metal contaminants in e-2- and mm-2-appended frameworks using inductively coupled plasma optical emission spectroscopy (ICP-OES) analysis, which revealed the presence of non-negligible amounts of Fe and Ni impurities (e.g., 15 and 1.6 ppm for Fe and Ni in e-2−Mg_2(dobpdc), respectively, corresponding to an Fe/Mg ratio of 0.007% and a Ni/Mg ratio of 0.0007%, Table S3), regardless of their oxidative stability.

To further evaluate the impact of minor metal impurities on the oxidative stability of diamine-appended frameworks, additional iron was doped into e-2−Mg_2(dobpdc) by preparing the Mg_2(dobpdc) framework with $Mg(NO_3)_2$ mixed with 3% of $FeCl_2$ (see the Supporting Information, Section S9 for detailed procedures). The resulting e-2−Mg_2(dobpdc), containing ∼2700 ppm of Fe (Fe/Mg ratio: 1.2%), degrades much faster in O_2 exposure experiments, as evidenced by DCl digestion studies (Figures S69 and S70) and CO_2 isobar measurements (Figure S72). For example, the e-2 loading of Fe-doped e-2−Mg_2(dobpdc) dropped from 90% to 22% after 5 days of O_2-exposure at 100 °C, while a decrease from 100% to 52% in e-2 loading was observed with non-Fe-doped e-2−Mg_2(dobpdc) under the identical exposure conditions (Figures S69 and S70 and Table S2). These results demonstrate that Fe species are detrimental to the oxidative stability of diamine-appended frameworks, supporting our hypothesis that a small amount of Fe (and possibly Ni) impurities in the adsorbent could cause the generation of radical species, such as peroxide radical anions or hydroxy radicals, which in turn initiate the degradation of amines.

Possible Degradation Pathways. Based on the mechanistic studies mentioned above and considering the possibility of C−N bond cleavage via C-centered radical pathways and the autoxidation mechanism reported in literature,[55,67] we propose a number of plausible pathways for O_2-induced degradation of e-2 within the pores of the framework, along with subsequent reactions (Figure 7). Given that multiple reactions occur both in parallel and sequentially during O_2 exposure, these pathways may not represent all degradation routes; however, they are the simplest that support formation of the species observed.

Figure 7 shows the degradation pathways for the e-2-appended frameworks with each framework type involving similar steps. Carbon-centered radical species can first be generated by a radical species ($A^\bullet$) produced from the reaction of trace metal with O_2 or oxidation of another e-2 molecule. Three types of C-centered radical species result in C−N bond cleavage, but the position of cleavage in the diamine differs (Figure 7a). Consequently, pathway 1 generates ethylamine and Mg−AA (AA = aminoacetaldehyde), while pathway 2 generates acetaldehyde and Mg−en. Indeed, the formation of ethylamine and acetaldehyde was confirmed by solid-state NMR and gas-phase mass spectrometry analyses, respectively. Pathway 3 generates ammonia that is bonded to the Mg site and ethylaminoacetaldehyde (AMA). Although AMA has not been detected in oxidized materials, this pathway cannot be simply ruled out, as calculations presented in following sections revealed that oxidation of AMA is both thermodynamically and kinetically feasible (Tables S7 and S9), and given the existence of multiple possible subsequent reactions of AMA, including the formation of AA.

Several degraded species mentioned above, such as Mg−AA and AMA, contain an aldehyde functionality that can be further oxidized to a carboxylic functionality or a carboxyl radical, followed by decarboxylation reactions to generate CO_2. As a typical example, Figure 7b (upper) outlines a pathway for CO_2 formation from the oxidation of Mg−AA, where an aminoacetic acid (glycine) radical can be formed to liberate CO_2. Formation of CO_2 during O_2 exposure has been confirmed by gas-phase mass spectrometry analyses; however, further studies are required to uncover whether a particular aldehyde source can selectively lead to CO_2 formation.

It is notable that the radical pathways follow a "chain-reaction"-like mechanism. Reactions of O_2 with any single radical species ($A^\bullet$) generate not only oxidized products (aldehydes, CO_2, etc.) but also three radical species ($A^\bullet$) that can subsequently react with O_2 (Figure 7a and 7b (th, lower)). In other words, it is crucial to prevent the spread of radical species within the pores of the frameworks to improve the oxidative stability.

In addition to successive oxidation processes, aldehyde species formed during O_2 exposure, such as Mg−AA, AMA, or glyoxal, may react with an amino functionality of a neighboring molecule, forming heavier species featuring imine functionalities. As shown in Figure 7c, there are some possible reactions between the oxidation products of e-2, or between e-2 and its oxidation products. Indeed, GC-MS studies indicate the formation of aldehyde species containing imine groups with mass-to-charge ratios of 128, 169, and 194.

Computational Studies of Oxidative Degradation Mechanisms. To complement experimental studies focusing

https://doi.org/10.1021/jacs.5c07551
J. Am. Chem. Soc. 2025, 147, 25761−25778

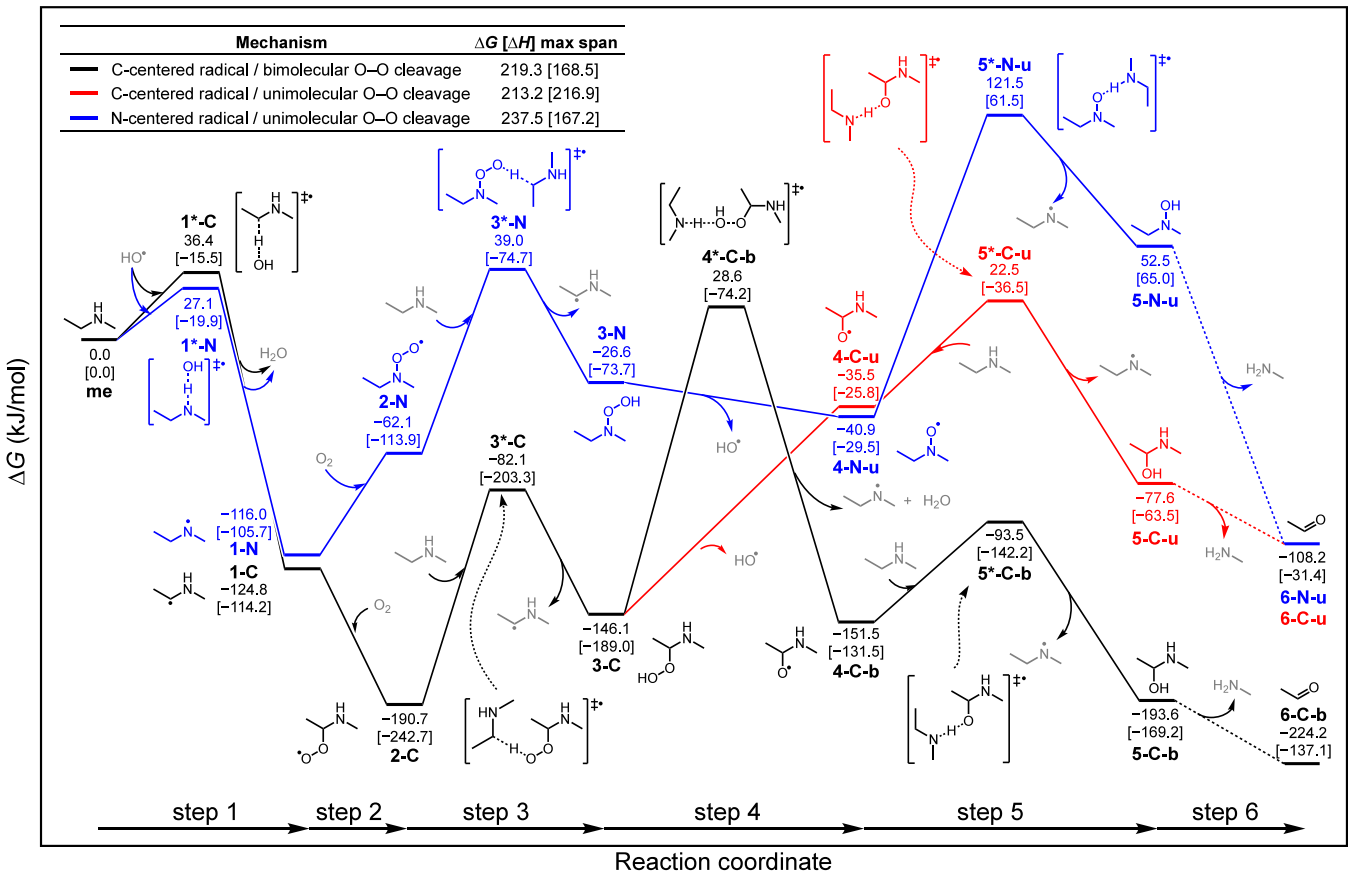

Figure 8. Computed reaction profile for the oxidative degradation of *N*-methylethylamine (**me**) as a simplified model for oxidative amine degradation (ωB97X-D3/def2-TZVPPD//ωB97X-D3/def2-SVP, thermochemistry calculated using the QRRHO approximation at 101,325 Pa (1 atm) and 100 °C). Changes in reaction free energy (Δ*G*) and enthalpy (Δ*H* in square brackets) are reported in kJ/mol. Species labeled in gray are reactants and products involved in degradation. Species involved in unimolecular and bimolecular O−O cleavage mechanisms are denoted with a **u** or **b** modifier to the compound symbol, respectively.

on product identification and specific mechanistic insights, computational approaches were used to understand quantitatively the energetics and mechanisms of the oxidative degradation of diamines within the frameworks.

Oxidation Mechanism for N-Methylethylamine. We first evaluated the energy landscape of the oxidative degradation of a model compound, *N*-methylethylamine, based on model reactions derived from our experimental observations (Figure 8). Static DFT calculations were carried out using Q-Chem (ver. 6.1)[76] at the ωB97X-D3/def2-TZVPPD//ωB97X-D3/def2-SVP level[77,78] with the QRRHO approximation at 100 °C and 1 atm (see the Supporting Information, Section S11.1 for details).[79,80]

The initiation reaction is modeled by the reaction of *N*-methylethylamine with OH•, forming a radical species (step 1). While this radical species could also be formed by other radicals (e.g., superoxide or peroxide), we presumed that the corresponding reaction profiles should be similar to those elaborated in Figure 8. A detailed discussion of possible initiation pathways is presented in the following sections. In step 1, N−H abstraction by OH• (blue path, $\Delta G^{\ddagger}$ = 27.1 kJ/mol) is found to be kinetically favored over C−H abstraction (black path, $\Delta G^{\ddagger}$ = 36.4 kJ/mol) at 100 °C, by 9.3 kJ/mol ($\Delta\Delta G^{\ddagger}$, or $\Delta\Delta H^{\ddagger}$ = 4.4 kJ/mol). However, the α-amino radical formed via C−H abstraction (**1-C**) is slightly more stable than the N-centered radical generated via N−H abstraction (**1-N**, $\Delta\Delta G$ = −8.8 kJ/mol, $\Delta\Delta H$ = −8.5 kJ/mol).

In the gas phase, C−O bond formation via trapping of the C-centered α-amino radical by triplet O_2 is expected to be strongly exergonic and exothermic (step 2, black path, ΔG = −65.9 kJ/mol, ΔH = −128.5 kJ/mol), while the weak N−O bond formed upon trapping of the N-centered radical results in an endergonic and mildly exothermic process (step 2, blue path, ΔG = +53.9 kJ/mol, ΔH = −8.2 kJ/mol). Therefore, even if the initial N−H abstraction (blue path) is favored over the C−H abstraction (black path), from the thermodynamic point of view, the subsequent C−O bond formation (black path) should be significantly favored over N−O bond formation (blue path). Assuming fast inter- or intramolecular radical translocation is allowed via hydrogen atom transfer (HAT, see the detailed discussion below), it is reasonable to assume that N-centered radicals induced by N−H abstraction can undergo translocation to form the C-centered radical (i.e., **1-C**), followed by reaction with O_2. The probability of radical translocation within the pores of the frameworks is described in the following sections.

Hydrogen atom transfer between **2-C** and a second equivalent of amine forms a hydroperoxyl species, 1-hydroperoxy-*N*-methylethan-1-amine (**3-C**, step 3). This reaction corresponds to the third step involved in the proposed degradation pathways of e-2 (Figure 7a). Cleavage of the O−O bond for this hydroperoxyl species may occur by either unimolecular homolytic fission to expel a hydroxyl radical (step 4, red path) or undergo bimolecular cleavage involving a third

https://doi.org/10.1021/jacs.5c07551
J. Am. Chem. Soc. 2025, 147, 25761−25778

N-methylethylamine molecule that liberates a water molecule (step 4, black path).[58] Quenching of the resulting O-centered radical (**4-C-u**) by HAT with an additional equivalent of amine generates an α-hydroxylamine (step 5, black/red paths), which may then undergo subsequent C−N bond cleavage to form acetaldehyde and methylamine (step 6, black/red paths).

In these gas phase model reactions, a competition between unimolecular and bimolecular O−O cleavage mechanisms may exist.[81−83] Our calculations revealed that the bimolecular pathway (black path) features a slightly higher rate-limiting free energy barrier (**2-C** → **4*-C-b**, $\Delta G^{\ddagger}$ = +219.3 kJ/mol), by 6.1 kJ/mol, than that of the unimolecular pathway (red path, **2-C** → **5*-C-u**, $\Delta G^{\ddagger}$ = +213.2 kJ/mol). In terms of enthalpy, however, the bimolecular pathway (black path, **2-C** → **4*-C-b**, $\Delta H^{\ddagger}$ = +168.5 kJ/mol) is strongly favored over the unimolecular pathway (black/red path, **2-C** → **4-C-u**, $\Delta H^{\ddagger}$ = +216.9 kJ/mol), by 48.4 kJ/mol. Further, acetaldehyde formation via the bimolecular pathway exhibits exergonicity with respect to the peroxyl radical intermediate (**2-C** → **6-C-b**, ΔG = −33.5 kJ/mol), while the formation of acetaldehyde via the unimolecular pathway (**6-C-u**) is endergonic compared with **2-C** (ΔG = +82.5 kJ/mol). The former is also far less endothermic compared to the latter (**2-C** → **6-C-b** vs **2-C** → **6-N/C-u**, ΔH = +105.6 kJ/mol vs +211.3 kJ/mol). Thus, we tentatively conclude that the bimolecular O−O cleavage mechanism is preferred for the oxidative degradation of *N*-methylethylamine in the gas phase and at elevated temperatures.

The energy landscape for *N*-methylethylamine oxidation via the N-centered pathway (blue path) was also evaluated. Starting from the N-centered radical species, **1-N**, the rate-limiting free energy barrier is found to be 237.5 kJ/mol (**2-N** → **5*-N-u**), which is higher than C-centered pathways (black or red path, 210−220 kJ/mol). This scenario suggests that the C-centered pathway is kinetically favored over the N-centered one.

Although our DFT calculations indicate that the oxidative degradation of gaseous diamines is thermodynamically feasible, we anticipate that the contribution of each mechanism to the overall degradation behaviors of diamines appended to the frameworks will vary strongly with temperature. This is because of the difference in the molecularity of the rate-limiting steps of the two competing C-centered radical pathways (i.e., unimolecular vs bimolecular pathways). We predict that the unimolecular process will dominate at higher temperatures due to the positive activation entropy of homolytic O−O bond fission ($\Delta S^{\ddagger}$ = +141 J/(mol·K)), compared with the negative activation entropy of bimolecular O−O cleavage ($\Delta S^{\ddagger}$ = −173 J/(mol·K)) and that the rate of amine degradation will accelerate with increasing temperature as a result.

In the realistic case involving amine oxidation in the frameworks, the confinement effects within the pores will substantially modify the entropic contributions to each of these mechanisms. Therefore, the difference in free energy observed with the simple *N*-methylethylamine model will not represent the actual scenario within the diamine-appended frameworks. For example, bimolecular processes such as **3-C** → **4*-C-b** are expected to be substantially accelerated under confinement. Additionally, coordination with the Lewis-acidic Mg^{2+} ion may impact amine decomposition (as discussed further below), and tunneling will increase the kinetic feasibility of transition states involving C−H cleavage. In addition, the involvement of multiple equivalents of amine is required in these "chain-reaction"-like mechanisms, and thus the balance of these processes is likely to be highly dependent on the amine used.

Three Diamine-MOF Models. To assess the impact of the framework environment on the initiation of the O_2-induced diamine degradation process, we modeled three diamine−framework clusters with different complexity (Figure 9a, see the Supporting Information, Section S11 for details). Among them, two cluster models, the **S** model and the **L** model were employed to understand the thermodynamics of HAT. The **S** model employed the $MgCl_2$ molecule to mimic the positively charged Mg^{2+} site. Although incapable of replicating the confinement effects induced by the framework pores, the simplicity of this model allows calculations with hybrid DFT. All calculations in this model were performed at the ωB97X-D3/def2-TZVPPD//ωB97X-D3/def2-SVP level of theory.

The **L** model was designed to replicate the actual environment surrounding the diamine in the framework. This model incorporates three adjacent diamines aligned along the *c* axis and a significant portion of the framework structure, including nine Mg atoms and ten truncated organic ligands (overall formula: $[(D)_3{-}Mg_9(salicylate)_9(benzoate)\text{-}(NH_3)_6(CH_3OH)_2]^{-}$) where D stands for a diamine. Due to the large size of this model, full optimization and consideration with hybrid DFT were impractical. A QM1/QM2 approach was therefore applied, where the target amine was described at the high QM1 level (ωB97X-D3/def2-TZVPPD//ωB97X-D3/def2-SVP), and the remaining atoms were included in the QM2 model (GFN2-xTB level).

The **M** model was used to investigate HAT kinetics. It employs three CH_2O ligands and a 2-oxybenzoate dianion to represent the organic linkers (overall formula: (D)-Mg-(salicylate)$(CH_2O)_3$). This model reproduces the octahedral coordination environment of the Mg^{2+} cation in the Mg-based frameworks more faithfully than the **S** model, despite not being able to replicate the steric environment around the diamine in the framework as precisely as the **L** model. The moderate size and complexity of this model allow the identification of corresponding transition states (TSs) using the ωB97X-D3/def2-TZVPPD//ωB97X-D3/def2-SVP level of theory without imposing any geometric constraints during optimization.

Thermodynamics of Initiation of the Degradation Process. As shown in Figures 7 and 8, we assume that the oxidative degradation of amines is initiated by the abstraction of a hydrogen atom by a radical species. To validate this assumption, elucidate the identity of potential initiators, and evaluate the susceptibility of selected diamines toward initiation (i.e., e-2, en, and mm-2), we calculated the thermodynamics associated with HAT at each C−H or N−H bond of the diamine appended to the Mg^{2+} sites (Figure 9b and Tables S5 and S6, see the Supporting Information for detailed discussions of computational subjects and methods) with the **S** and **L** models. More specifically, we calculated the differences in Gibbs free energies and electronic energies for hydrogen atom detachments ($R{-}H \rightarrow R^{\bullet} + H^{\bullet}$) at all possible C−H or N−H bonds of the diamine to estimate the energy required to remove a hydrogen atom from the diamine. In addition, we calculated the differences in Gibbs free energies and electronic energies for the radical quenching reaction ($X + H^{\bullet} \rightarrow X{-}H^{\bullet}$ for X = O_2 (*S* = 0 or 1) and O_2^{-}, and $X^{\bullet} + H^{\bullet} \rightarrow X{-}H$ for X = $OH^{\bullet}$). The combination of energies for these two reactions allows us to determine which attacking radical

https://doi.org/10.1021/jacs.5c07551
J. Am. Chem. Soc. 2025, 147, 25761−25778

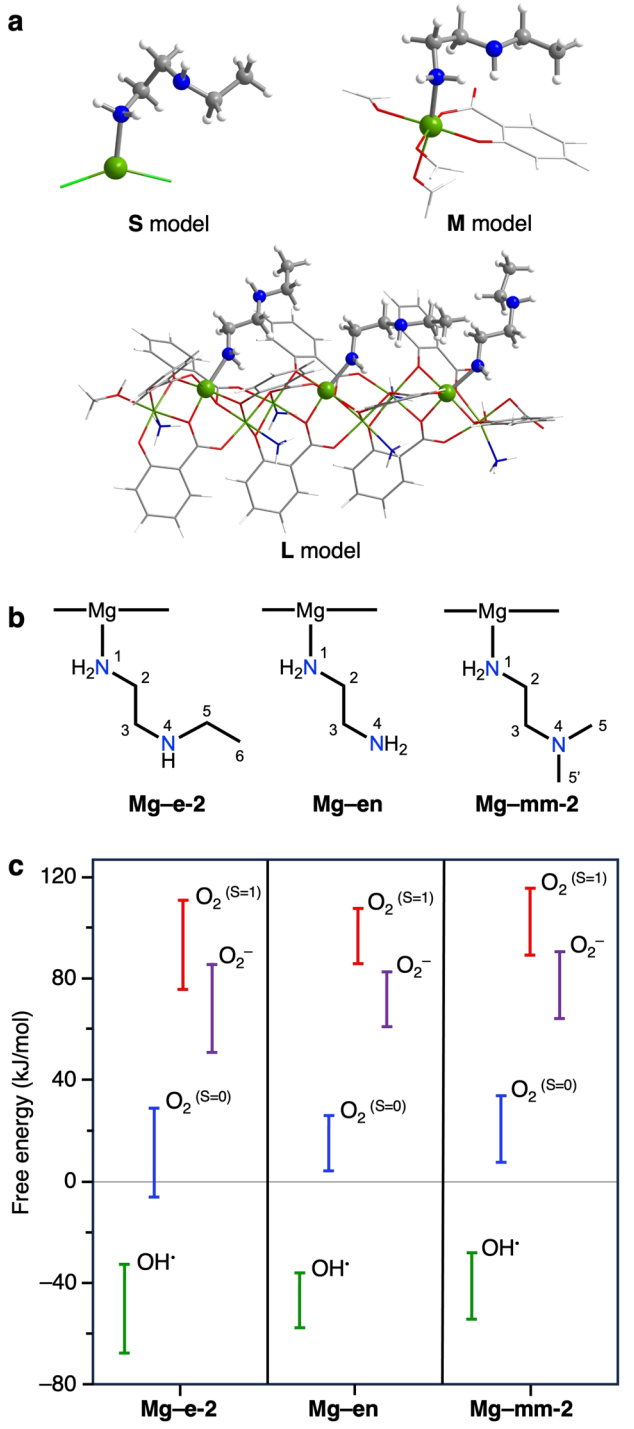

Figure 9. (a) DFT optimized structures of diamine–MOF clusters. Green, gray, red, blue, pale green, and white represent Mg, C, O, N, Cl, and H atoms, respectively. The diamine molecules and the Mg atoms to which the diamines are coordinated are shown as ball-and-stick models. Other units are shown in wire-and-stick for clarity. (b) Numbering of the C and N atoms in three diamines. (c) Thermodynamics of initiation of the degradation process depicted by the differences in Gibbs free energies for HAT between different attacking radical species and different diamines using the **L** model. The range indicates the values for different attacked C–H and N–H bonds. See Table S5 for values for all cases.

species could yield an overall exergonic HAT reaction (R–H + $X^{\bullet}$ → X–H + $R^{\bullet}$ or R–H + X → X–$H^{\bullet}$ + $R^{\bullet}$).

As a typical example, Figure 9c depicts the range of differences in Gibbs free energies for HAT between different attacking radical species and all possible C–H and N–H bonds at different diamines using the **L** model. For three diamines, e-2, en, and mm-2, initiation by triplet O_2 (red) and superoxide (purple) were found to be strongly disfavored thermodynamically. Initiation by singlet O_2 (blue) lies on the border of thermodynamic feasibility; however, experiments carried out in the absence of light rule out triplet oxygen sensitization as the major initiation mechanism. In all cases, initiation by hydroxyl radical is predicted to be thermodynamically favored. One possible pathway for the formation of the hydroxyl radical involves the reaction of a trace amount of metal impurities (e.g., iron and nickel) with O_2 to generate hydroxy radicals.[74] Considering that Fe and Ni impurities were detected in the diamine-appended frameworks, it is likely that at least one of the plausible initiation pathways involves the hydroxyl radicals induced by these metal impurities.

Comparison of the differences in Gibbs free energies for hydrogen atom detachments (R–H → $R^{\bullet}$ + $H^{\bullet}$) at all possible C–H or N–H bonds of the diamine also allows us to evaluate the relative thermodynamic stability of the radical species with the radical located at different C or N atoms (Table S5). Notably, the N-centered radicals are generally less stable than the C-centered radicals, being about 40 kJ/mol higher in energy than the most stable C-centered radical, in both **S** and **L** models. For the C-centered radicals, coordination to the Mg^{2+} site destabilizes the formation of a radical at sites closest to the metal atom (i.e., site **2**, Figure 9b). For example, the radical located at site 2 of e-2 is destabilized by approximately 20–30 kJ/mol with respect to the most stable sites (i.e., sites **3** and **5**). In addition, the primary β-amino C-centered radical at site **6** remains less stable than those α-amino C-centered radicals at sites **3** and **5** for both bare and coordinated e-2 (Table S5). Consequently, sites **3** and **5** are more thermodynamically favorable for forming C-centered radicals than other sites. Similar trends were observed for diamines en and mm-2 (Table S5). In this context, removing all α-amino hydrogen atoms could improve resistance toward oxidation, as it prevents the formation of the most stable α-amino C-centered radicals. This is indeed supported by experimental results, where high oxidative stability was observed by appending the framework with tmen due to the full substitution of protons adjacent to the nitrogen atoms with methyl functionalities.

Kinetics of Initiation of the Degradation Process. Although the thermodynamic data highlight the stability of certain radicals, kinetic barriers play a crucial role in determining the preferred site for HAT initiation via the initial $OH^{\bullet}$ radical attack. Therefore, we performed constrained molecular dynamics simulations (see the Supporting Information, Section S12.2 for details) to analyze the kinetics of the HAT process. Specifically, the distance between the oxygen atom of the $OH^{\bullet}$ radical and the hydrogen atom of the C–H or N–H moieties, as well as the C–H or N–H bond lengths, were identified as the key distances. These distances were determined from the typical transition state geometries involving the C–H or N–H moieties and kept constant throughout the simulation.

We found that H atom abstraction is kinetically feasible at both C–H and N–H sites (Figure S81). Notably, when the diamine is coordinated with the positively charged Mg site, the barrier for the HAT process at sites **1** and **2** generally increases (Figures S82 and S83). Further, the mean energy from

https://doi.org/10.1021/jacs.5c07551
J. Am. Chem. Soc. 2025, 147, 25761–25778

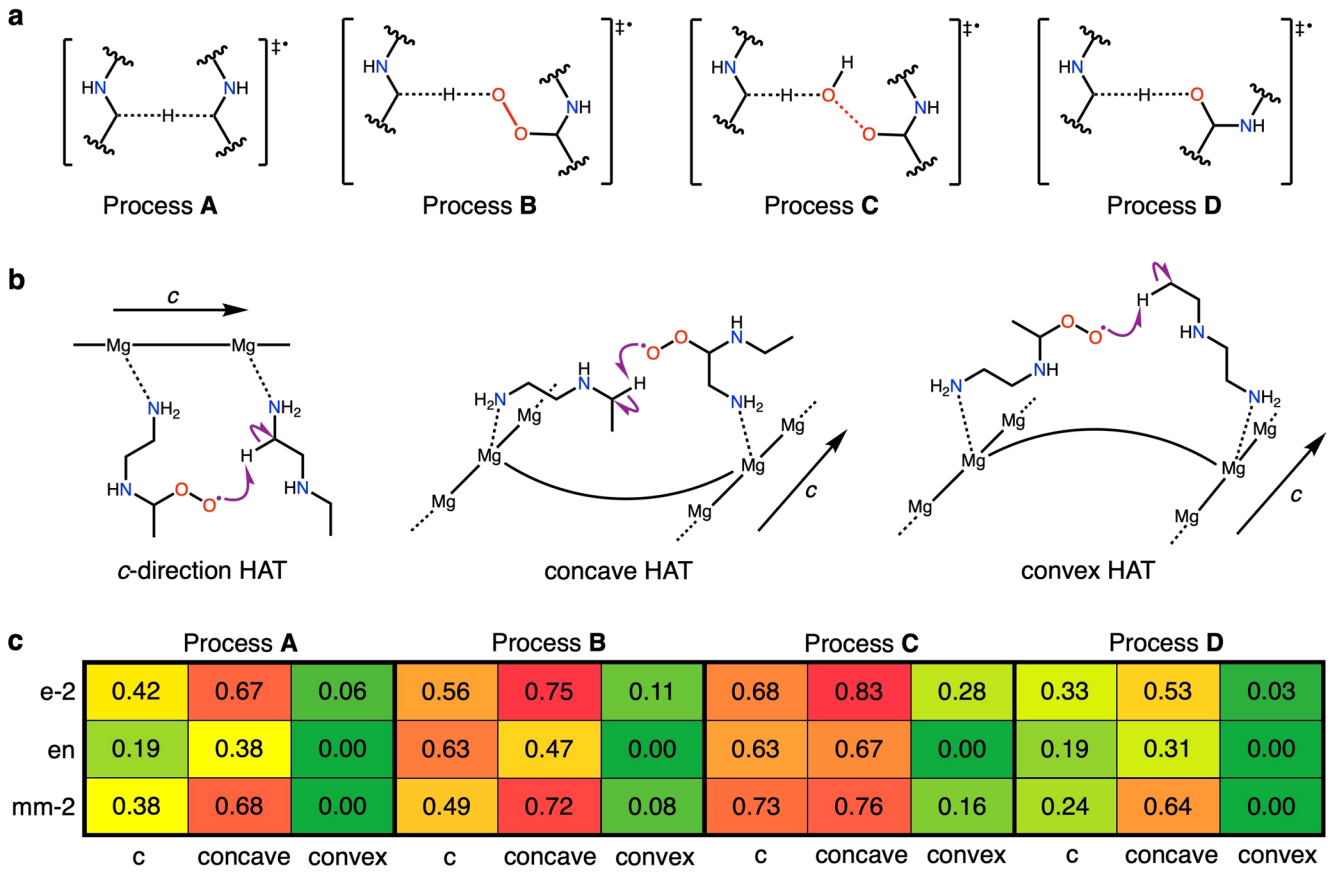

c

	Process A			Process B			Process C			Process D		
	c	concave	convex	c	concave	convex	c	concave	convex	c	concave	convex
e-2	0.42	0.67	0.06	0.56	0.75	0.11	0.68	0.83	0.28	0.33	0.53	0.03
en	0.19	0.38	0.00	0.63	0.47	0.00	0.63	0.67	0.00	0.19	0.31	0.00
mm-2	0.38	0.68	0.00	0.49	0.72	0.08	0.73	0.76	0.16	0.24	0.64	0.00

Figure 10. (a) Four scenarios for the hydrogen atom transfer (HAT) process with a neighboring diamine. (b) Three possible HAT pathways with the neighboring amino group located in three directions (illustrated using process B as an example). (c) Likelihood indexes of degradation of the neighboring amino functionality in the framework pores, calculated using **LC** models. A number approaching unity indicates a greater chance of HAT.

constrained molecular dynamics suggests a moderately lower activation barrier for HAT at site **4** (N−H site) than at adjacent sites **3** and **5** (two C−H sites). This aligns with the computational results for the *N*-methylethylamine model (Figure 8), which is indicative of a lower activation barrier for N−H abstraction compared with C−H abstraction. These results imply that the amino functionality with one or more hydrogen atoms, farthest from the positive charge, is the favored site for the HAT initiation from a kinetic perspective. Conversely, the tertiary nitrogen atom at site **4** in mm-2 hinders the rapid formation of the N-centered radicals. This feature could account for the high oxidative stability of mm-2-appended frameworks.

Additionally, we performed static calculations with the **M** model. The results indicate that the barriers to HAT are low ($\Delta G^{\ddagger} \simeq 20-40$ kJ/mol, Table S8), suggesting rapid initiation kinetics following $OH^{\bullet}$ formation. This model serves as a valuable estimation of the magnitudes of activation barriers that can be expected in the considered HAT reaction, even though the **M** model cannot differentiate among various HAT sites due to its smaller cluster size. With that said, after the rapid formation of a C-centered or N-centered radical, subsequent radical shifts are likely to lead to the formation of an ensemble of the most stable α-amino C-centered radicals, which then participate in subsequent reactions as discussed below.

Propagation Mechanisms and the Likelihood Index for Radical Transfer to Neighboring Diamines. As depicted in Figure 7a, upon formation of the C-centered radicals in the framework, most of them are likely to undergo HAT processes with a neighboring amino species (process A, Figure 10a) or react with O_2 to generate an α-peroxylamine radical. The hydrogen atom transfer from the α-peroxylamine radical to a neighboring amino species (process B) will form a new C-centered or N-centered radical on the neighboring amino species and quench the O-centered radical to form a hydroperoxyamine. The resulting hydroperoxyamine can subsequently undergo bimolecular HAT with a neighboring amino species (process C) to generate another new C-centered radical and an alkoxy radical. This alkoxy radical can also undergo HAT with a neighboring amino species (process D) to produce a third C-centered radical. The latter three processes (B−D) involve amplifying "chain-reaction"-like propagation, where the reaction of one C-centered radical with one O_2 molecule generates three additional C-centered radical species.

For these four HAT processes (A−D), the abstracted proton is likely to be transferred to a neighboring diamine along the pore (*c* axis) or a diamine coordinated to the neighboring one-dimensional $Mg_3(O)_3(CO_2)_3$ rod (Figure 10b). Considering that the hexagonal channel of Mg_2(dobpdc) is somewhat distorted, the edge of the hexagon can be termed concave or convex. Similar to the **L** model, a set of cluster models (**LC** models) was developed to reproduce the environment surrounding the diamine along the *c* axis, from the concave direction, and from the convex direction of the framework

https://doi.org/10.1021/jacs.5c07551
J. Am. Chem. Soc. 2025, 147, 25761−25778

pores (Figure S79, see the Supporting Information, Section S11.4 for more details). A likelihood index was developed using a composite approach consisting of molecular dynamics simulations and statistical analysis to evaluate the likelihood of HAT processes with neighboring diamines from different directions (see the Supporting Information, Sections S11.4 and S13 for details). Briefly, the likelihood index ranges from 0 to 1 and a higher likelihood index indicates a greater chance of HAT with respect to the distance. A process is considered "feasible" if the likelihood index is larger than 0.50.

For the HAT process A (Figure 10a), these calculations suggest that equilibration by HAT with neighboring amines is feasible for e-2- and mm-2-appended Mg_2(dobpdc) frameworks, as shown by their likelihood indexes of up to 0.67 and 0.68 (Figure 10c); however, it is slightly less likely for en−Mg_2(dobpdc) which features a shorter diamine. For all of the diamine-appended Mg_2(dobpdc) frameworks studied, the HAT processes B and C should be possible, given the corresponding likelihood indexes for the three diamines are up to 0.63−0.83 (Figure 10c). The neighboring diamine could be an adjacent diamine across the concave edge of the hexagonal channel or along the *c* axis. Transfer of a hydrogen atom across the convex face of the framework is more difficult for processes A−C, as indicated by the relatively low values of corresponding likelihood indexes (0−0.28) compared to that of HAT along the *c* axis (0.19−0.73) and across the concave face (0.31−0.83). This is potentially due to the increased interamine distance.

In the case of process D, HAT with a neighboring amine across the concave edge of the hexagonal channel can be possible for the alkoxy radicals derived from both e-2 and mm-2. In contrast, HAT involving the alkoxy radical derived from en and a neighboring amine is predicted to be slow due to its shorter length compared to e-2 and mm-2. In this context, we envision that frameworks appended with shorter diamines or frameworks with larger pore sizes and/or longer distances between metal sites along the *c* axis would exhibit higher oxidative stability. These structural characteristics could provide two benefits: (i) the oxidized diamine itself would have to undergo an alternative, higher-energy (i.e., slower) degradation pathway, and (ii) the radical propagation of nearby amines would be hindered. On the other hand, these characteristics could also result in weakened cooperativity, amine volatilization and/or lower volumetric CO_2 adsorption capacities, and thus it is important to balance the benefits of enhanced oxidative stability with the potential trade-offs in performance.

CONCLUSIONS AND OUTLOOK

Oxygen-involved degradation of diamines appended in magnesium-based metal−organic frameworks was extensively investigated. The results indicate that O_2 exposure leads to amine degradation, accompanied by the formation of acetaldehyde, carbon dioxide, water, ethylamine, and other aldehyde- and imine-containing species. Notably, the molecular structures of the products of O_2-induced degradation have not yet been conclusively identified for other amine-based adsorbents, including silica- or alumina-supported amine adsorbents.[31,37,48−59,84,85] Diamine degradation through radical-induced C−N bond cleavage ultimately inhibits CO_2 chemisorption and, consequently, causes a loss of CO_2 adsorption capacity. With computational support, we propose detailed degradation mechanisms. It was found that oxidation is likely to be initiated by $OH^•$, followed by the N-centered radical formation. These N-centered radicals will be converted to C-centered radicals through fast intra- or intermolecular H atom translocation to undergo subsequent "chain-reaction"-like oxidative degradation. Importantly, this work also revealed that the amine structure significantly impacts the rate of oxidative degradation by affecting the selectivity and barrier of O−O cleavage and HAT processes.

These findings support several strategies for inhibiting the detrimental impact of O_2 on CO_2 capture technologies with diamine-appended frameworks: (1) Considering that frameworks such as Mg_2(dobpdc) and Mg_2(olz) exhibit much greater stability to O_2 exposure than diamines, degraded adsorbents may be recycled by replacing damaged diamines (Figure S73). A preliminary demonstration of this concept was included in the Supporting Information (Section S10). For both e-2−Mg_2(dobpdc) and e-2−Mg_2(olz), the recycled materials exhibited similar profiles of CO_2 isobars, including their step temperature and adsorption capacity, compared with the corresponding pristine materials (Figures S76 and S77). Ultimately, this approach could extend the service life of the bare frameworks and thus reduce the cost of materials in carbon capture. (2) Oxygen-induced degradation of diamines can be initiated by hydroxyl radicals that could be generated through the reaction of O_2 with trace amounts of transition metal impurities such as iron. Therefore, ensuring that the diamine-appended frameworks have minimal levels of transition metal contamination and/or performing adsorption−desorption cycles in equipment or containers that preclude the presence of redox-active components should improve the oxidative stability of the adsorbents. Note, however, that this would likely be associated with increases in costs, required steps, and complexity of the overall setup. (3) Given the favored amine H atom abstraction by $OH^•$, primary, tertiary (1°,3°) diamine-appended frameworks should exhibit higher oxidative stability. Indeed, O_2 exposure experiments showed a much smaller impact on the loss of the CO_2 adsorption capacity for mm-2-appended frameworks compared to e-2-appended ones. It should be recognized, however, that primary, tertiary diamine-appended frameworks (e.g., mm-2−Mg_2(olz) and ee-2−Mg_2(dobpdc), ee-2 = *N*,*N*-diethylethylenediamine) are typically not capable of capturing CO_2 from very dilute CO_2 streams.[20,22] (4) Degradation of diamines via C-centered pathways can be suppressed by substituting protons on the carbon atoms adjacent to the nitrogen atoms with alkyl groups. While adsorbents containing such rigid and bulky diamines may not be suitable for cooperative CO_2 capture—as evidenced by tmen−Mg_2(olz), which showed negligible CO_2 chemisorption capacity under 1 bar of CO_2 (Figure S65)—innovative material design could circuvent this limitation and result in high-performance, oxidatively stable, and cost-effective adsorbents. We envision that such materials will be identified soon.

ASSOCIATED CONTENT

Supporting Information

The Supporting Information is available free of charge at https://pubs.acs.org/doi/10.1021/jacs.5c07551.

Detailed experimental procedures, characterizations of the reported compounds, gas adsorption data, additional spectroscopic data, supplemental experimental studies, and computational information (PDF)

https://doi.org/10.1021/jacs.5c07551
J. Am. Chem. Soc. 2025, 147, 25761−25778

Cartesian coordinates of the optimized structures of each cluster model and initial structures used to generate molecular dynamics simulation data (ZIP)

AUTHOR INFORMATION

Corresponding Authors

Martin Head-Gordon − *Institute for Decarbonization Materials, Pitzer Center for Theoretical Chemistry, and Department of Chemistry, University of California, Berkeley, California 94720, United States; Chemical Sciences Division, Lawrence Berkeley National Laboratory, Berkeley, California 94720, United States;* orcid.org/0000-0002-4309-6669; Email: m_headgordon@berkeley.edu

Jeffrey R. Long − *Institute for Decarbonization Materials, Department of Chemistry, Department of Chemical and Biomolecular Engineering, and Department of Materials Science and Engineering, University of California, Berkeley, California 94720, United States; Materials Sciences Division, Lawrence Berkeley National Laboratory, Berkeley, California 94720, United States;* orcid.org/0000-0002-5324-1321; Email: jrlong@berkeley.edu

Authors

Shuoyan Xiong − *Institute for Decarbonization Materials and Department of Chemistry, University of California, Berkeley, California 94720, United States; Materials Sciences Division, Lawrence Berkeley National Laboratory, Berkeley, California 94720, United States;* orcid.org/0000-0002-2579-4260

Alistair J. Sterling − *Pitzer Center for Theoretical Chemistry and Department of Chemistry, University of California, Berkeley, California 94720, United States; Chemical Sciences Division, Lawrence Berkeley National Laboratory, Berkeley, California 94720, United States;* Present Address: Department of Chemistry & Biochemistry, The University of Texas at Dallas, Richardson, Texas 75080, United States (A.J.S.); orcid.org/0000-0002-3571-1094

Nikolay V. Tkachenko − *Institute for Decarbonization Materials, Pitzer Center for Theoretical Chemistry, and Department of Chemistry, University of California, Berkeley, California 94720, United States; Materials Sciences Division, Lawrence Berkeley National Laboratory, Berkeley, California 94720, United States;* orcid.org/0000-0002-7296-4293

Rhea-Donna Reyes − *Institute for Decarbonization Materials and Department of Chemistry, University of California, Berkeley, California 94720, United States*

Hsinhan Tsai − *Institute for Decarbonization Materials and Department of Chemistry, University of California, Berkeley, California 94720, United States; Materials Sciences Division, Lawrence Berkeley National Laboratory, Berkeley, California 94720, United States;* Present Address: Department of Chemical and Biological Engineering, The State University of New York at Buffalo, Buffalo, New York 14260, United States (H.T.).; orcid.org/0000-0002-1492-1279

Jaeheon Lee − *Department of Chemical and Biomolecular Engineering, University of California, Berkeley, California 94720, United States; Energy Storage and Distributed Resources Division, Lawrence Berkeley National Laboratory, Berkeley, California 94720, United States;* orcid.org/0000-0002-9285-0728

Yu Chen − *Department of Materials Science and Engineering, University of California, Berkeley, California 94720, United States; Molecular Foundry, Lawrence Berkeley National Laboratory, Berkeley, California 94720, United States;* orcid.org/0000-0002-5420-7571

Yang Wang − *Institute for Decarbonization Materials and Department of Chemical and Biomolecular Engineering, University of California, Berkeley, California 94720, United States*

Matthew N. Dods − *Institute for Decarbonization Materials and Department of Chemical and Biomolecular Engineering, University of California, Berkeley, California 94720, United States; Materials Sciences Division, Lawrence Berkeley National Laboratory, Berkeley, California 94720, United States*

David Lu − *Department of Chemistry, University of California, Berkeley, California 94720, United States*

Ziting Zhu − *Institute for Decarbonization Materials and Department of Materials Science and Engineering, University of California, Berkeley, California 94720, United States; Materials Sciences Division, Lawrence Berkeley National Laboratory, Berkeley, California 94720, United States;* orcid.org/0000-0002-4173-0347

Jonas Börgel − *Department of Chemistry, University of California, Berkeley, California 94720, United States; Materials Sciences Division, Lawrence Berkeley National Laboratory, Berkeley, California 94720, United States;* orcid.org/0000-0001-5301-8579

Jeong Won Kim − *Institute for Decarbonization Materials and Department of Materials Science and Engineering, University of California, Berkeley, California 94720, United States; Materials Sciences Division, Lawrence Berkeley National Laboratory, Berkeley, California 94720, United States*

Abigail J. Schmeiser − *Department of Chemical and Biomolecular Engineering, University of California, Berkeley, California 94720, United States*

Junyang Meng − *Institute for Decarbonization Materials and Department of Chemistry, University of California, Berkeley, California 94720, United States*

Hiroyasu Furukawa − *Institute for Decarbonization Materials and Department of Chemistry, University of California, Berkeley, California 94720, United States; Materials Sciences Division, Lawrence Berkeley National Laboratory, Berkeley, California 94720, United States;* orcid.org/0000-0002-6082-1738

Aaron W. Peters − *ExxonMobil Technology and Engineering Company, Annandale, New Jersey 08801, United States*

Bryan D. McCloskey − *Department of Chemical and Biomolecular Engineering, University of California, Berkeley, California 94720, United States; Energy Storage and Distributed Resources Division, Lawrence Berkeley National Laboratory, Berkeley, California 94720, United States;* orcid.org/0000-0001-6599-2336

Jeffrey A. Reimer − *Institute for Decarbonization Materials and Department of Chemical and Biomolecular Engineering, University of California, Berkeley, California 94720, United States; Materials Sciences Division, Lawrence Berkeley National Laboratory, Berkeley, California 94720, United States*

Simon C. Weston − *ExxonMobil Technology and Engineering Company, Annandale, New Jersey 08801, United States;* orcid.org/0000-0002-7439-5055

Complete contact information is available at: https://pubs.acs.org/10.1021/jacs.5c07551

https://doi.org/10.1021/jacs.5c07551
J. Am. Chem. Soc. 2025, 147, 25761−25778

Author Contributions

†S.X., A.J.S., and N.V.T. contributed equally to this work.

Notes

The authors declare no competing financial interest.

■ ACKNOWLEDGMENTS

This research was supported by ExxonMobil Technology and Engineering Company. We thank Dr. Joseph Falkowski, Dr. Henry Jiang, Katerina Graf, Dr. Kurtis Carsch, Dr. Benjamin Snyder, Adrian Huang, Dr. Sophia Fricke, Dr. Mengshan Ye, and Dr. Gen Li for insightful discussions. We thank Dr. Hasan Celik, Dr. Raynald Giovine, and the Pines Magnetic Resonance Center's Core NMR Facility (PMRC Core) for spectroscopic assistance. The instruments used in this work were supported by the PMRC Core and the National Science Foundation under Grant No. 2018784. The computational work was supported by the U.S. Department of Energy, Office of Science, Office of Basic Energy Sciences, under Contract No. DE-AC02-05CH11231 with Lawrence Berkeley National Laboratory, and Scientific Discovery through Advanced Computing (SciDAC) program (M.H.G.). Support for A.J.Schmeiser was provided by the Amgen Scholars Program.

■ REFERENCES

(1) National Oceanic and Atmospheric Administration *Trends in Atmospheric Carbon Dioxide*. http://www.esrl.noaa.gov/gmd/ccgg/trends/ (accessed January 21, 2025).
(2) Masson-Delmotte, V.; Zhai, P.; Pirani, A.; Connors, S. L.; Péan, C.; Berger, S.; Caud, N.; Chen, Y.; Goldfarb, L.; Gomis, M. *IPCC 2021: Climate Change 2021: The Physical Science Basis. Contribution of Working Group I to the Sixth Assessment Report of the Intergovernmental Panel on Climate Change*; Cambridge Univ. Press: New York, 2021.
(3) Siegelman, R. L.; Kim, E. J.; Long, J. R. Porous Materials for Carbon Dioxide Deparations. *Nat. Mater.* **2021**, *20* (8), 1060−1072.
(4) Majumdar, A.; Deutch, J. Research Opportunities for CO_2 Utilization and Negative Emissions at the Gigatonne Scale. *Joule* **2018**, *2* (5), 805−809.
(5) Haszeldine, R. S. Carbon Capture and Storage: How Green Can Black Be? *Science* **2009**, *325* (5948), 1647−1652.
(6) Chu, S. Carbon Capture and Sequestration. *Science* **2009**, *325* (5948), 1599−1599.
(7) Sanz-Perez, E. S.; Murdock, C. R.; Didas, S. A.; Jones, C. W. Direct Capture of CO_2 from Ambient Air. *Chem. Rev.* **2016**, *116* (19), 11840−11876.
(8) Bui, M.; Adjiman, C. S.; Bardow, A.; Anthony, E. J.; Boston, A.; Brown, S.; Fennell, P. S.; Fuss, S.; Galindo, A.; Hackett, L. A.; Hallett, J. P.; Herzog, H. J.; Jackson, G.; Kemper, J.; Krevor, S.; Maitland, G. C.; Matuszewski, M.; Metcalfe, I. S.; Petit, C.; Puxty, G.; Reimer, J.; Reiner, D. M.; Rubin, E. S.; Scott, S. A.; Shah, N.; Smit, B.; Trusler, J. P. M.; Webley, P.; Wilcox, J.; Mac Dowell, N. Carbon Capture and Storage (CCS): The Way Forward. *Energy Environ. Sci.* **2018**, *11* (5), 1062−1176.
(9) Erans, M.; Sanz-Pérez, E. S.; Hanak, D. P.; Clulow, Z.; Reiner, D. M.; Mutch, G. A. Direct Air Capture: Process Technology, Techno-Economic and Socio-Political Challenges. *Energy Environ. Sci.* **2022**, *15* (4), 1360−1405.
(10) Dutcher, B.; Fan, M.; Russell, A. G. Amine-Based CO_2 Capture Technology Development from the Beginning of 2013— A Review. *ACS Appl. Mater. & Interfaces* **2015**, *7* (4), 2137−2148.
(11) Wang, S.; Yan, S.; Ma, X.; Gong, J. Recent Advances in Capture of Carbon Dioxide Using Alkali-Metal-Based Oxides. *Energy Environ. Sci.* **2011**, *4* (10), 3805−3819.
(12) Choi, S.; Drese, J. H.; Jones, C. W. Adsorbent Materials for Carbon Dioxide Capture from Large Anthropogenic Point Sources. *ChemSusChem* **2009**, *2* (9), 796−854.
(13) Dziejarski, B.; Serafin, J.; Andersson, K.; Krzyzynska, R. CO_2 Capture Materials: A Review of Current Trends and Future Challenges. *Mater. Today Sustain.* **2023**, *24*, No. 100483.
(14) Zhu, X.; Xie, W.; Wu, J.; Miao, Y.; Xiang, C.; Chen, C.; Ge, B.; Gan, Z.; Yang, F.; Zhang, M.; O'Hare, D.; Li, J.; Ge, T.; Wang, R. Recent Advances in Direct Air Capture by Adsorption. *Chem. Soc. Rev.* **2022**, *51* (15), 6574−6651.
(15) McDonald, T. M.; Lee, W. R.; Mason, J. A.; Wiers, B. M.; Hong, C. S.; Long, J. R. Capture of Carbon Dioxide from Air and Flue Gas in the Alkylamine-Appended Metal−Organic Framework mmen-Mg_2(dobpdc). *J. Am. Chem. Soc.* **2012**, *134* (16), 7056−7065.
(16) Siegelman, R. L.; Milner, P. J.; Forse, A. C.; Lee, J. H.; Colwell, K. A.; Neaton, J. B.; Reimer, J. A.; Weston, S. C.; Long, J. R. Water Enables Efficient CO_2 Capture from Natural Gas Flue Emissions in an Oxidation-Resistant Diamine-Appended Metal−Organic Framework. *J. Am. Chem. Soc.* **2019**, *141* (33), 13171−13186.
(17) Siegelman, R. L.; Thompson, J. A.; Mason, J. A.; McDonald, T. M.; Long, J. R. A Cooperative Adsorbent for the Switch-Like Capture of Carbon Dioxide from Crude Natural Gas. *Chem. Sci.* **2022**, *13* (40), 11772−11784.
(18) Milner, P. J.; Martell, J. D.; Siegelman, R. L.; Gygi, D.; Weston, S. C.; Long, J. R. Overcoming Double-Step CO_2 Adsorption and Minimizing Water Co-Adsorption in Bulky Diamine-Appended Variants of Mg_2(dobpdc). *Chem. Sci.* **2018**, *9* (1), 160−174.
(19) Siegelman, R. L.; McDonald, T. M.; Gonzalez, M. I.; Martell, J. D.; Milner, P. J.; Mason, J. A.; Berger, A. H.; Bhown, A. S.; Long, J. R. Controlling Cooperative CO_2 Adsorption in Diamine-Appended Mg_2(dobpdc) Metal−Organic Frameworks. *J. Am. Chem. Soc.* **2017**, *139* (30), 10526−10538.
(20) Milner, P. J.; Siegelman, R. L.; Forse, A. C.; Gonzalez, M. I.; Runcevski, T.; Martell, J. D.; Reimer, J. A.; Long, J. R. A Diaminopropane-Appended Metal−Organic Framework Enabling Efficient CO_2 Capture from Coal Flue Gas via a Mixed Adsorption Mechanism. *J. Am. Chem. Soc.* **2017**, *139* (38), 13541−13553.
(21) Kim, E. J.; Siegelman, R. L.; Jiang, H. Z. H.; Forse, A. C.; Lee, J. H.; Martell, J. D.; Milner, P. J.; Falkowski, J. M.; Neaton, J. B.; Reimer, J. A.; Weston, S. C.; Long, J. R. Cooperative Carbon Capture and Steam Regeneration with Tetraamine-Appended Metal−Organic Frameworks. *Science* **2020**, *369* (6502), 392−396.
(22) Zhu, Z.; Parker, S. T.; Forse, A. C.; Lee, J. H.; Siegelman, R. L.; Milner, P. J.; Tsai, H.; Ye, M.; Xiong, S.; Paley, M. V.; Uliana, A. A.; Oktawiec, J.; Dinakar, B.; Didas, S. A.; Meihaus, K. R.; Reimer, J. A.; Neaton, J. B.; Long, J. R. Cooperative Carbon Dioxide Capture in Diamine-Appended Magnesium−Olsalazine Frameworks. *J. Am. Chem. Soc.* **2023**, *145* (31), 17151−17163.
(23) McDonald, T. M.; Mason, J. A.; Kong, X.; Bloch, E. D.; Gygi, D.; Dani, A.; Crocella, V.; Giordanino, F.; Odoh, S. O.; Drisdell, W. S.; Vlaisavljevich, B.; Dzubak, A. L.; Poloni, R.; Schnell, S. K.; Planas, N.; Lee, K.; Pascal, T.; Wan, L. F.; Prendergast, D.; Neaton, J. B.; Smit, B.; Kortright, J. B.; Gagliardi, L.; Bordiga, S.; Reimer, J. A.; Long, J. R. Cooperative Insertion of CO_2 in Diamine-Appended Metal−Organic Frameworks. *Nature* **2015**, *519* (7543), 303−308.
(24) Lee, W. R.; Hwang, S. Y.; Ryu, D. W.; Lim, K. S.; Han, S. S.; Moon, D.; Choi, J.; Hong, C. S. Diamine-Functionalized Metal−Organic Framework: Exceptionally High CO_2 Capacities from Ambient Air and Flue Gas, Ultrafast CO_2 Uptake Rate, and Adsorption Mechanism. *Energy Environ. Sci.* **2014**, *7* (2), 744−751.
(25) Lee, W. R.; Jo, H.; Yang, L. M.; Lee, H.; Ryu, D. W.; Lim, K. S.; Song, J. H.; Min, D. Y.; Han, S. S.; Seo, J. G.; Park, Y. K.; Moon, D.; Hong, C. S. Exceptional CO_2 Working Capacity in a Heterodiamine-Grafted Metal−Organic Framework. *Chem. Sci.* **2015**, *6* (7), 3697−3705.
(26) Choe, J. H.; Kim, H.; Kang, M.; Yun, H.; Kim, S. Y.; Lee, S. M.; Hong, C. S. Functionalization of Diamine-Appended MOF-Based Adsorbents by Ring Opening of Epoxide: Long-Term Stability and CO_2 Recyclability under Humid Conditions. *J. Am. Chem. Soc.* **2022**, *144* (23), 10309−10319.
(27) Bose, S.; Sengupta, D.; Malliakas, C. D.; Idrees, K. B.; Xie, H.; Wang, X.; Barsoum, M. L.; Barker, N. M.; Dravid, V. P.; Islamoglu, T.;

https://doi.org/10.1021/jacs.5c07551
J. Am. Chem. Soc. 2025, 147, 25761−25778

Farha, O. K. Suitability of a Diamine Functionalized Metal−Organic Framework for Direct Air Capture. *Chem. Sci.* **2023**, *14* (35), 9380−9388.
(28) Choe, J. H.; Kim, H.; Yun, H.; Kurisingal, J. F.; Kim, N.; Lee, D.; Lee, Y. H.; Hong, C. S. Extended MOF-74-Type Variant with an Azine Linkage: Efficient Direct Air Capture and One-Pot Synthesis. *J. Am. Chem. Soc.* **2024**, *146* (28), 19337−19349.
(29) Xu, J.; Liu, Y. M.; Lipton, A. S.; Ye, J. X.; Hoatson, G. L.; Milner, P. J.; McDonald, T. M.; Siegelman, R. L.; Forse, A. C.; Smit, B.; Long, J. R.; Reimer, J. A. Amine Dynamics in Diamine-Appended Mg_2(dobpdc) Metal−Organic Frameworks. *J. Phys. Chem. Lett.* **2019**, *10* (22), 7044−7049.
(30) Forse, A. C.; Milner, P. J.; Lee, J. H.; Redfearn, H. N.; Oktawiec, J.; Siegelman, R. L.; Martell, J. D.; Dinakar, B.; Zasada, L. B.; Gonzalez, M. I.; Neaton, J. B.; Long, J. R.; Reimer, J. A. Elucidating CO_2 Chemisorption in Diamine-Appended Metal−Organic Frameworks. *J. Am. Chem. Soc.* **2018**, *140* (51), 18016−18031.
(31) Lashaki, M. J.; Khiavi, S.; Sayari, A. Stability of Amine-Functionalized CO_2 Adsorbents: a Multifaceted Puzzle. *Chem. Soc. Rev.* **2019**, *48* (12), 3320−3405.
(32) Arasto, A.; Tsupari, E.; Kärki, J.; Pisilä, E.; Sorsamäki, L. Post-Combustion Capture of CO_2 at an Integrated Steel Mill - Part I: Technical Concept Analysis. *Int. J. Greenhouse Gas Control* **2013**, *16*, 271−277.
(33) Zevenhoven, R.; Kilpinen, P. *Control of Pollutants in Flue Gases and Fuel Gases*; Picaset Oy: Finland, N. p., 2001.
(34) Dods, M. N.; Kim, E. J.; Long, J. R.; Weston, S. C. Deep CCS: Moving Beyond 90% Carbon Dioxide Capture. *Environ. Sci. Technol.* **2021**, *55* (13), 8524−8534.
(35) Raganati, F.; Miccio, F.; Ammendola, P. Adsorption of Carbon Dioxide for Post-Combustion Capture: A Review. *Energy Fuels* **2021**, *35* (16), 12845−12868.
(36) Patel, H. A.; Byun, J.; Yavuz, C. T. Carbon Dioxide Capture Adsorbents: Chemistry and Methods. *ChemSusChem* **2017**, *10* (7), 1303−1317.
(37) Carneiro, J. S. A.; Innocenti, G.; Moon, H. J.; Guta, Y.; Proaño, L.; Sievers, C.; Sakwa-Novak, M. A.; Ping, E. W.; Jones, C. W. Insights into the Oxidative Degradation Mechanism of Solid Amine Sorbents for CO_2 Capture from Air: Roles of Atmospheric Water. *Angew. Chem. Int. Ed.* **2023**, *62* (24), No. e202302887.
(38) Uyanga, I. J.; Idem, R. O. Studies of SO_2- and O_2-Induced Degradation of Aqueous MEA During CO_2 Capture from Power Plant Flue Gas Streams. *Ind. Eng. Chem. Res.* **2007**, *46* (8), 2558−2566.
(39) Lepaumier, H.; Picq, D.; Carrette, P.-L. New Amines for CO_2 Capture. II. Oxidative Degradation Mechanisms. *Ind. Eng. Chem. Res.* **2009**, *48* (20), 9068−9075.
(40) Lepaumier, H.; Picq, D.; Carrette, P.-L. New Amines for CO_2 Capture. I. Mechanisms of Amine Degradation in the Presence of CO_2. *Ind. Eng. Chem. Res.* **2009**, *48* (20), 9061−9067.
(41) Supap, T.; Idem, R.; Tontiwachwuthikul, P.; Saiwan, C. Kinetics of Sulfur Dioxide- and Oxygen-Induced Degradation of Aqueous Monoethanolamine Solution During CO_2 Absorption from Power Plant Flue Gas Streams. *Int. J. Greenhouse Gas Control* **2009**, *3* (2), 133−142.
(42) Wang, T.; Jens, K.-J. Oxidative Degradation of Aqueous 2-Amino-2-Methyl-1-Propanol Solvent for Postcombustion CO_2 Capture. *Ind. Eng. Chem. Res.* **2012**, *51* (18), 6529−6536.
(43) Fredriksen, S.; Jens, K.-J. Oxidative Degradation of Aqueous Amine Solutions of MEA, AMP, MDEA, Pz: A Review. *Energy Procedia* **2013**, *37*, 1770−1777.
(44) Bougie, F.; Iliuta, M. C. Stability of Aqueous Amine Solutions to Thermal and Oxidative Degradation in the Absence and the Presence of CO_2. *Int. J. Greenhouse Gas Control* **2014**, *29*, 16−21.
(45) Vevelstad, S. J.; Buvik, V.; Knuutila, H. K.; Grimstvedt, A.; da Silva, E. F. Important Aspects Regarding the Chemical Stability of Aqueous Amine Solvents for CO_2 Capture. *Ind. Eng. Chem. Res.* **2022**, *61* (43), 15737−15753.
(46) Yang, X.; Tao, Y.; Murphy, J. G. Kinetics of the Oxidation of Ammonia and Amines with Hydroxyl Radicals in the Aqueous phase. *Environ. Sci.: Processes. Impacts* **2021**, *23* (12), 1906−1913.
(47) Meng, F.; Meng, Y.; Ju, T.; Han, S.; Lin, L.; Jiang, J. Research Progress of Aqueous Amine Solution for CO_2 Capture: A Review. *Renew. Sustain. Energy Rev.* **2022**, *168*, No. 112902.
(48) Pang, S. H.; Lively, R. P.; Jones, C. W. Oxidatively-Stable Linear Poly(propylenimine)-Containing Adsorbents for CO_2 Capture from Ultradilute Streams. *ChemSusChem* **2018**, *11* (15), 2628−2637.
(49) Miao, Y. H.; Wang, Y. Z.; Zhu, X. C.; Chen, W.; He, Z. J.; Yu, L. J.; Li, J. Minimizing the Effect of Oxygen on Supported Polyamine for Direct Air Capture. *Sep. Purif. Technol.* **2022**, *298*, No. 121583.
(50) Rosu, C.; Pang, S. H.; Sujan, A. R.; Sakwa-Novak, M. A.; Ping, E. W.; Jones, C. W. Effect of Extended Aging and Oxidation on Linear Poly(propylenimine)-Mesoporous Silica Composites for CO_2 Capture from Simulated Air and Flue Gas Streams. *ACS Appl. Mater. Interfaces* **2020**, *12* (34), 38085−38097.
(51) Miao, Y.; Wang, Y.; Ge, B.; He, Z.; Zhu, X.; Li, J.; Liu, S.; Yu, L. Mixed Diethanolamine and Polyethyleneimine with Enhanced CO_2 Capture Capacity from Air. *Adv. Sci.* **2023**, *10* (16), No. 2207253.
(52) Bali, S.; Chen, T. T.; Chaikittisilp, W.; Jones, C. W. Oxidative Stability of Amino Polymer-Alumina Hybrid Adsorbents for Carbon Dioxide Capture. *Energy Fuels* **2013**, *27* (3), 1547−1554.
(53) Ahmadalinezhad, A.; Sayari, A. Oxidative Degradation of Silica-Supported Polyethylenimine for CO_2 Adsorption: Insights into the Nature of Deactivated Species. *Phys. Chem. Chem. Phys.* **2014**, *16* (4), 1529−1535.
(54) Heydari-Gorji, A.; Belmabkhout, Y.; Sayari, A. Degradation of Amine-Supported CO_2 Adsorbents in the Presence of Oxygen-Containing Gases. *Microporous Mesoporous Mater.* **2011**, *145* (1−3), 146−149.
(55) Nezam, I.; Xie, J. W.; Golub, K. W.; Carneiro, J.; Olsen, K.; Ping, E. W.; Jones, C. W.; Sakwa-Novak, M. A. Chemical Kinetics of the Autoxidation of Poly(ethylenimine) in CO_2 Sorbents. *ACS Sustain. Chem. Eng.* **2021**, *9* (25), 8477−8486.
(56) Racicot, J.; Li, S. C.; Clabaugh, A.; Hertz, C.; Akhade, S. A.; Ping, E. W.; Pang, S. H.; Sakwa-Novak, M. A. Volatile Products of the Autoxidation of Poly(ethylenimine) in CO_2 Sorbents. *J. Phys. Chem. C* **2022**, *126* (20), 8807−8816.
(57) Buijs, W. CO_2 Capture with PEI: A Molecular Modeling Study of the Ultimate Oxidation Stability of LPEI and BPEI. *ACS Eng. Au* **2023**, *3* (1), 28−36.
(58) Li, S.; Cerón, M. R.; Eshelman, H. V.; Varni, A. J.; Maiti, A.; Akhade, S.; Pang, S. H. Probing the Kinetic Origin of Varying Oxidative Stability of Ethyl- vs. Propyl- spaced Amines for Direct Air Capture. *ChemSusChem* **2023**, *16* (5), No. e202201908.
(59) Didas, S. A.; Zhu, R. S.; Brunelli, N. A.; Sholl, D. S.; Jones, C. W. Thermal, Oxidative and CO_2 Induced Degradation of Primary Amines Used for CO_2 Capture: Effect of Alkyl Linker on Stability. *J. Phys. Chem. C* **2014**, *118* (23), 12302−12311.
(60) Hefti, M.; Joss, L.; Bjelobrk, Z.; Mazzotti, M. On the Potential of Phase-Change Adsorbents for CO_2 Capture by Temperature Swing Adsorption. *Faraday Discuss.* **2016**, *192*, 153−179.
(61) Huck, J. M.; Lin, L. C.; Berger, A. H.; Shahrak, M. N.; Martin, R. L.; Bhown, A. S.; Haranczyk, M.; Reuter, K.; Smit, B. Evaluating Different Classes of Porous Materials for Carbon Capture. *Energy Environ. Sci.* **2014**, *7* (12), 4132−4146.
(62) Eggert, H.; Djerassi, C. Carbon-13 Nuclear Magnetic Resonance Spectra of Acyclic Aliphatic Amines. *J. Am. Chem. Soc.* **1973**, *95* (11), 3710−3718.
(63) Borthakur, I.; Joshi, A.; Kumari, S.; Kundu, S. Metal-Free Visible-Light Induced Oxidative Cleavage of $C(sp^3)$−C, and $C(sp^3)$−N Bonds of Nitriles, Alcohols, and Amines. *Chem. - Eur. J.* **2024**, *30* (14), No. e202303295.
(64) Iqbal, N.; Cho, E. J. Formation of Carbonyl Compounds from Amines through Oxidative C−N Bond Cleavage using Visible Light Photocatalysis and Applications to *N*-PMB-Amide Deprotection. *Adv. Synth. Catal.* **2015**, *357* (10), 2187−2192.

https://doi.org/10.1021/jacs.5c07551
J. Am. Chem. Soc. 2025, 147, 25761−25778

(65) Fulmer, G. R.; Miller, A. J. M.; Sherden, N. H.; Gottlieb, H. E.; Nudelman, A.; Stoltz, B. M.; Bercaw, J. E.; Goldberg, K. I. NMR Chemical Shifts of Trace Impurities: Common Laboratory Solvents, Organics, and Gases in Deuterated Solvents Relevant to the Organometallic Chemist. *Organometallics* **2010**, *29* (9), 2176−2179.
(66) Lewis, F. D.; Ho, T. I.; Simpson, J. T. Photochemical Addition of Tertiary-Amines to Stilbene-Free-Radical and Electron-Transfer Mechanisms for Amine Oxidation. *J. Am. Chem. Soc.* **1982**, *104* (7), 1924−1929.
(67) Bedell, S. A. Oxidative Degradation Mechanisms for Amines in Flue Gas Capture. *Greenhouse Gas Control Technol.* **2009**, *1* (1), 771−778.
(68) Silverman, R. B.; Hoffman, S. J.; Catus, W. B. A Mechanism for Mitochondrial Monoamine-Oxidase Catalyzed Amine Oxidation. *J. Am. Chem. Soc.* **1980**, *102* (23), 7126−7128.
(69) Lewis, F. D.; Simpson, J. T. Free-Radical and Electron-Transfer Mechanisms for Tertiary Amine Oxidation. *J. Am. Chem. Soc.* **1980**, *102* (25), 7593−7595.
(70) Rochelle, G.; Chi, S. Oxidative Degradation of Aqueous MEA in Capture Systems under Absorber Conditions. *Ind. Eng. Chem. Res.* **2002**, *41*, 4178−4186.
(71) Voice, A. K.; Closmann, F.; Rochelle, G. T. Oxidative Degradation of Amines with High-Temperature Cycling. *Ghgt-11* **2013**, *37*, 2118−2132.
(72) Min, K.; Choi, W.; Kim, C.; Choi, M. Rational Design of the Polymeric Amines in Solid Adsorbents for Postcombustion Carbon Dioxide Capture. *ACS Appl. Mater. Interfaces* **2018**, *10* (28), 23825−23833.
(73) Min, K.; Choi, W.; Kim, C.; Choi, M. Oxidation-Stable Amine-Containing Adsorbents for Carbon Dioxide Capture. *Nat. Commun.* **2018**, *9* (1), 726.
(74) Voice, A. K.; Rochelle, G. T. Oxidation of Amines at Absorber Conditions for CO_2 Capture from Flue Gas. *Energy Procedia* **2011**, *4*, 171−178.
(75) Buijs, W. Direct Air Capture of CO_2 with an Amine Resin: A Molecular Modeling Study of the Oxidative Deactivation Mechanism with O_2. *Ind. Eng. Chem. Res.* **2019**, *58* (38), 17760−17767.
(76) Epifanovsky, E.; Gilbert, A. T. B.; Feng, X.; Lee, J.; Mao, Y.; Mardirossian, N.; Pokhilko, P.; White, A. F.; Coons, M. P.; Dempwolff, A. L.; Gan, Z.; Hait, D.; Horn, P. R.; Jacobson, L. D.; Kaliman, I.; Kussmann, J.; Lange, A. W.; Lao, K. U.; Levine, D. S.; Liu, J.; McKenzie, S. C.; Morrison, A. F.; Nanda, K. D.; Plasser, F.; Rehn, D. R.; Vidal, M. L.; You, Z. Q.; Zhu, Y.; Alam, B.; Albrecht, B. J.; Aldossary, A.; Alguire, E.; Andersen, J. H.; Athavale, V.; Barton, D.; Begam, K.; Behn, A.; Bellonzi, N.; Bernard, Y. A.; Berquist, E. J.; Burton, H. G. A.; Carreras, A.; Carter-Fenk, K.; Chakraborty, R.; Chien, A. D.; Closser, K. D.; Cofer-Shabica, V.; Dasgupta, S.; de Wergifosse, M.; Deng, J.; Diedenhofen, M.; Do, H.; Ehlert, S.; Fang, P. T.; Fatehi, S.; Feng, Q.; Friedhoff, T.; Gayvert, J.; Ge, Q.; Gidofalvi, G.; Goldey, M.; Gomes, J.; González-Espinoza, C. E.; Gulania, S.; Gunina, A. O.; Hanson-Heine, M. W. D.; Harbach, P. H. P.; Hauser, A.; Herbst, M. F.; Hernández Vera, M.; Hodecker, M.; Holden, Z. C.; Houck, S.; Huang, X.; Hui, K.; Huynh, B. C.; Ivanov, M.; Jász, Á.; Ji, H.; Jiang, H.; Kaduk, B.; Kähler, S.; Khistyaev, K.; Kim, J.; Kis, G.; Klunzinger, P.; Koczor-Benda, Z.; Koh, J. H.; Kosenkov, D.; Koulias, L.; Kowalczyk, T.; Krauter, C. M.; Kue, K.; Kunitsa, A.; Kus, T.; Ladjánszki, I.; Landau, A.; Lawler, K. V.; Lefrancois, D.; Lehtola, S.; Li, R. R.; Li, Y. P.; Liang, J.; Liebenthal, M.; Lin, H. H.; Lin, Y. S.; Liu, F.; Liu, K. Y.; Loipersberger, M.; Luenser, A.; Manjanath, A.; Manohar, P.; Mansoor, E.; Manzer, S. F.; Mao, S. P.; Marenich, A. V.; Markovich, T.; Mason, S.; Maurer, S. A.; McLaughlin, P. F.; Menger, M. F. S. J.; Mewes, J. M.; Mewes, S. A.; Morgante, P.; Mullinax, J. W.; Oosterbaan, K. J.; Paran, G.; Paul, A. C.; Paul, S. K.; Pavošević, F.; Pei, Z.; Prager, S.; Proynov, E. I.; Rák, Á.; Ramos-Cordoba, E.; Rana, B.; Rask, A. E.; Rettig, A.; Richard, R. M.; Rob, F.; Rossomme, E.; Scheele, T.; Scheurer, M.; Schneider, M.; Sergueev, N.; Sharada, S. M.; Skomorowski, W.; Small, D. W.; Stein, C. J.; Su, Y. C.; Sundstrom, E. J.; Tao, Z.; Thirman, J.; Tornai, G. J.; Tsuchimochi, T.; Tubman, N. M.; Veccham, S. P.; Vydrov, O.; Wenzel, J.; Witte, J.; Yamada, A.; Yao, K.; Yeganeh, S.; Yost, S. R.; Zech, A.; Zhang, I. Y.; Zhang, X.; Zhang, Y.; Zuev, D.; Aspuru-Guzik, A.; Bell, A. T.; Besley, N. A.; Bravaya, K. B.; Brooks, B. R.; Casanova, D.; Chai, J. D.; Coriani, S.; Cramer, C. J.; Cserey, G.; DePrince, A. E.; DiStasio, R. A.; Dreuw, A.; Dunietz, B. D.; Furlani, T. R.; Goddard, W. A.; Hammes-Schiffer, S.; Head-Gordon, T.; Hehre, W. J.; Hsu, C. P.; Jagau, T. C.; Jung, Y.; Klamt, A.; Kong, J.; Lambrecht, D. S.; Liang, W.; Mayhall, N. J.; McCurdy, C. W.; Neaton, J. B.; Ochsenfeld, C.; Parkhill, J. A.; Peverati, R.; Rassolov, V. A.; Shao, Y.; Slipchenko, L. V.; Stauch, T.; Steele, R. P.; Subotnik, J. E.; Thom, A. J. W.; Tkatchenko, A.; Truhlar, D. G.; Van Voorhis, T.; Wesolowski, T. A.; Whaley, K. B.; Woodcock, H. L.; Zimmerman, P. M.; Faraji, S.; Gill, P. M. W.; Head-Gordon, M.; Herbert, J. M.; Krylov, A. I. Software for the Frontiers of Quantum hemistry: An Overview of Developments in the Q-Chem 5 Package. *J. Chem. Phys.* **2021**, *155* (8), No. 084801.
(77) Lin, Y.-S.; Li, G.-D.; Mao, S.-P.; Chai, J.-D. Long-Range Corrected Hybrid Density Functionals with Improved Dispersion Corrections. *J. Chem. Theory Comput.* **2013**, *9* (1), 263−272.
(78) Weigend, F.; Ahlrichs, R. Balanced Basis Sets of Split Valence, Triple Zeta Valence and Quadruple Zeta Valence Quality for H to Rn: Design and Assessment of Accuracy. *Phys. Chem. Chem. Phys.* **2005**, *7* (18), 3297−3305.
(79) Grimme, S. Supramolecular Binding Thermodynamics by Dispersion-Corrected Density Functional Theory. *Chem. - Eur. J.* **2012**, *18* (32), 9955−9964.
(80) Li, Y. P.; Gomes, J.; Mallikarjun Sharada, S.; Bell, A. T.; Head-Gordon, M. Improved Force-Field Parameters for QM/MM Simulations of the Energies of Adsorption for Molecules in Zeolites and a Free Rotor Correction to the Rigid Rotor Harmonic Oscillator Model for Adsorption Enthalpies. *J. Phys. Chem. C* **2015**, *119* (4), 1840−1850.
(81) Spier, E.; Neuenschwander, U.; Hermans, I. Insights into the Cobalt (II)-Catalyzed Decomposition of Peroxide. *Angew. Chem., Int. Ed.* **2013**, *52* (5), 1581−1585.
(82) Zeng, X.; Zhang, X.; Wang, Z. Theoretical Study on the OH-Initiated Oxidation Mechanism of Polyfluorinated Dibenzo-p-Dioxins under the Atmospheric Conditions. *Chemosphere* **2016**, *144*, 2036−2043.
(83) Suh, I.; Zhao, J.; Zhang, R. Unimolecular Decomposition of Aromatic Bicyclic Alkoxy Radicals and Their Acyclic Radicals. *Chem. Phys. Lett.* **2006**, *432* (1−3), 313−320.
(84) Bhown, A. S.; Freeman, B. C. Analysis and Status of Post-Combustion Carbon Dioxide Capture Technologies. *Environ. Sci. & Technol.* **2011**, *45* (20), 8624−8632.
(85) Si, W.; Yang, B.; Yu, Q.; Lei, L.; Zhu, J. Deactivation Kinetics of Polyethylenimine-based Adsorbents Used for the Capture of Low Concentration CO_2. *ACS Omega* **2019**, *4* (6), 11237−11244.

https://doi.org/10.1021/jacs.5c07551
J. Am. Chem. Soc. 2025, 147, 25761−25778